Heliyon 10 (2024) e27919

Contents lists available at ScienceDirect

Heliyon

journal homepage: www.cell.com/heliyon

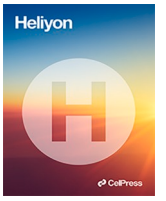

Research article

Rainfall trends and spatiotemporal patterns of meteorological drought in Menna watershed, northwestern Ethiopia

Fekadie Bazie Enyew [a], Simachew Bantigegn Wassie [b,*]

[a] Department of Geography and Environmental Studies, Kebri Dehar University, P.O. Box 250, Kebri Dehar, Ethiopia
[b] Department of geography and environmental studies, Bahir Dar University, P.O. Box 79, Bahir Dar, Ethiopia

ARTICLE INFO

Keywords:
CHIRPS rainfall
Drought indices
Meteorological drought
Rainfall trends
Menna watershed
Ethiopia

ABSTRACT

Understanding the spatiotemporal patterns of drought is crucial for planning, disaster preparedness, vulnerability assessment, impact evaluation, and policy formulation to mitigate drought-induced effects. The purpose of this study was to assess rainfall trends and spatiotemporal patterns of meteorological drought using geospatial techniques in Menna watershed. The Climate Hazards Group InfraRed Precipitation with Stations (CHIRPS) rainfall, and station-based observed rainfall were the datasets used. The station-based rainfall was used to confirm the accuracy of CHIRPS rainfall data. The Mann-Kendall (MK) test and Sen's slope estimator were utilized to assess trends and ascertain the extent of change. To characterize meteorological droughts, percent of normal (PN), standardized anomaly index (SAI), and standardized precipitation index (SPI) were computed during the crop growing seasons (2000–2022). The validation result confirmed a strong agreement between the observed and CHIRPS rainfall data ($R2 = 0.88$). Based on the MK test, an increasing trend has been observed in annual (3.7 mm/year) and *belg* (3.4 mm/year) rainfall, which was significant at $p < 0.05$. But the *kiremt* season was slightly decreasing (−0.7 mm/year). The PN, SAI, and SPI values detected that 2002, 2004, 2009, 2011, 2014, 2015, and 2019 were drought years in the area. Even only 1.4, 0.2, and 0.5% of the watershed were free from drought in 2009, 2014, and 2015, respectively, due to extremely high rainfall deficiency. Conversely, 2001, 2010, and 2016 were notable for having the highest amounts of rainfall compared to the other years. Generally, the region could be classified as an area highly susceptible to meteorological drought in northwestern Ethiopia. There was no even a single year free from drought in the entire study period. To that extent, about 86% of it had repeatedly encountered extreme rainfall deficit (7–23 times) during the study period. Thus, the population has always been repeatedly smashed down by the frequent droughts. To tackle existing challenges and mitigate upcoming risks, continual droughts monitoring and implementation of efficient early warning systems are vital for the region.

1. Introduction

Drought is a highly complex natural hazard that has substantial environmental, social, and economic effects on a worldwide scale [1]. It is a recurring extreme climate event, which varies overtime and space in its onset, intensity, duration and areal coverage [2]. Currently, around 50% of the Earth's land area is at risk of experiencing drought [3]. Hence, several drought events are recurring in

* Corresponding author.
E-mail addresses: fekadiebazie03@gmail.com (F.B. Enyew), simyebb@gmail.com (S.B. Wassie).

https://doi.org/10.1016/j.heliyon.2024.e27919
Received 12 December 2023; Received in revised form 25 February 2024; Accepted 8 March 2024
Available online 9 March 2024

different parts of the world [4]. The IPCC recently confirmed that climate extremes such as droughts are projected to get worse in the future due to anticipated climate change, impacting the livelihoods and well-being of the world population [5]. Though difficult to quantify and most figures are deep underestimates, annual losses from direct costs that droughts are causing in USA reach $6.4 billion and the European Union some €9.0 billion. Such figures would be larger and killed a huge number of people each year in less capable nations [6].

Drought is a prevalent climate-related hazard throughout much of the African continent [3,7]. In the last 50 years, the continent has experienced an increased drought frequency, intensity, and areal coverage, often with disastrous outcomes, subjecting the population to food insecurity and other socio-economic and environmental adversities [8]. Particularly, East African countries are extremely vulnerable to the impacts of recurring droughts and associated challenges because of significant variability in rainfall patterns [9,10]. In 1984, a devastating drought occurred in the area, resulting in the deaths of approximately 450,000 individuals in only Ethiopia and Sudan. Similarly, in June 2011, severe drought conditions in Somalia and Southern Ethiopia affected over 10 million people, leading to the need for humanitarian assistance and prompting 380,000 refugees to seek shelter in neighboring nations [11]. During July 2011 and mid-2012, the entire East African region experienced a severe drought. Such droughts, the most severe in six decades, have resulted in significant food shortages throughout Somalia, Djibouti, Ethiopia, and Kenya, putting the livelihoods of 9.5 million individuals at risk [12]. The United Nations Office for the Coordination of Humanitarian Affairs (UNOCHA) recently reported that approximately 36.4 million individuals have been impacted by the longest and most severe drought of 2022 in the Horn of Africa. Among these, the largest share of affected population (24.1 million) were in Ethiopia, the remaining 7.8, and 4.5 million were in Somalia and Kenya, respectively [13].

Ethiopia, one among the East African nations, is at high risk of drought in almost all regions [14]. Drought continues to be the primary source of disasters and human suffering in Ethiopia, impacting various aspects of people's lives [1,8]. Currently, Ethiopia experiences regular drought occurrences, with incidents happening every two to three years [15]. These crises were typically accompanied by famine, social complications, and political unrest [16].

Northwestern Ethiopia, where this study was conducted, often experiences recurrent droughts and is recognized as one of the food-insecure areas in the Amhara Region. In such impoverished areas, agriculture is conducted under the challenge of unpredictable rainfall patterns and is frequently impacted by recurring droughts, which are often succeeded by severe famines [17]. In line with this, the Water for Food Security, Women Empowerment, and Environment Protection Project (SWEEP) indicated that the East and West Belesa woredas are regions at risk of disasters, facing regular drought occurrences. During 2016, about 27% of the communities were under the support of Productive Safety Net Program (PSNP) due to the recurring droughts. Additionally, the community in Belesa (West 20.4% and East 34%) received assistance through emergency food aid, and 9% of them rely on water rations for eight months annually. The community in the Menna Watershed relies heavily on rain-fed agriculture for their livelihood. Unfortunately, the frequent droughts and resulting crop failures are a prevalent issue, as agriculture only offers a minimal amount of food to meet the needs of the quickly expanding population in the region.

Drought-related organizational reports noted that Menna watershed is categorized among areas with stressed food insecurity situation due to the impact of multi-year droughts, where food access remains limited for millions of households (http://earlywarning.usgs.gov/fews/reports.php). The zonal agriculture office also reported that substantial amount of crop yield has been lost each year due to rainfall deficit and recurring drought events. Variations in rainfall patterns have impacted the spatial and temporal spread of runoff, soil moisture, and groundwater levels. As a result, droughts persist and their effects have become more severe. Accordingly, meteorological condition that later propagate into agricultural droughts could easily and extremely affect the agriculture sector in the area [8]. Anticipated future alterations in the timing and distribution of precipitation are likely to impact the types of crops grown and the overall agricultural output in the area [18]. Therefore, it is essential to study the spatial distribution and changes of rainfall over time, along with tracking the historical patterns of meteorological drought in the region. This kind of analysis is critical for effective water resource management, enhancing agricultural productivity, and addressing drought-related concerns.

Several studies in existing literature focus on evaluating and observing drought conditions in the surrounding regions of the Menna watershed at a local scale in Ethiopia. According to Gebre et al. [19] employed NDVI, VCI, and SPEI to characterize droughts in North Wollo Zone. Similarly, Wassie et al. [18] applied Z-score index (SAI) and LST to characterize meteorological droughts in that area. In addition, Senamaw et al. [20] used SPI, NDVI and VCI in Waghmarea zone. Except few, many of them depend on station-based observed rainfall data to detect droughts. Analyzing drought using only this data is challenging because it lacks adequate spatial and temporal details, potentially leading to an incomplete understanding of historical drought trends and their associated impacts [21]. Other studies have also been carried out on the analysis of rainfall patterns and variations, encompassing various spatial and temporal scales [8,16,22,23]. Many of such studies did not see how the spatiotemporal variation of rainfall cussed the historical droughts in their study site. Therefore, this study tried to fill such gaps and address the issues by analyzing the trend and variability of rainfall and determining the onset, cessation and length of the rainy seasons with historic meteorological drought valuations using geospatial technologies at a watershed level.

The primary aim of this research was, therefore, to assess the precipitation trends and spatiotemporal characteristics of meteorological drought in the Menna watershed through the application of geospatial methods. Analyzing drought characteristics on a local level has important implications for effective drought management, including the development of early warning systems for climate-induced hazards, early warning system and intervention planning, and climate change adaptation initiatives [24]. Liou and Mulualem [25] also noted that better analysis and improved understanding of climate extremes, such as droughts, facilitate the development and execution of effective policies to comprehend the effects of climate change, enhance the food security system, and fortify communities that are resilient to it.

2. Materials and methods

2.1. Study area

The study was carried-out in Menna Watershed, which is part of Tekeze river basin located between 12°20′33″ N to 13°15′57″ N and 37°33′52″ E to 38°21′2″ E in Amhara National Regional state (ANRS). It covers about seven *woredas* of North Gondar Zone such as, Wogera, Janamora, Gondar zuria, Dabat, Debark, east and west Belesa. It covers an estimated area of 5242.6 km^2 having diverse topographic features with elevations that ranges from 1239 to 4418 m.a.s.l (Fig. 1).

The area contains four distinct agro-ecological zones: lowland (*Kolla*), midland (*Woina-dega*), highland (*Dega*), and cold (*Wurch*), which encompass 3.9%, 58%, 33.5%, and 4.6% of the total area, respectively [26,27]. Such different agro-ecologies are very important for agricultural practices allowing farmers to diversify crop types and raise their production [28]. The average annual precipitation and average annual temperature in the research area are 984.2 mm and 18.9 °C, respectively. Therefore, Menna watershed is located in the tropical climate type which receives main rainfall during *kiremt* season (June–September). In the area, the largest share of the landscape (63.5%) is covered by rangelands followed by crop lands (32%), whereas forests, water bodies and bare lands cover the smallest area covering 0.8, 0.1 and 0.02%, respectively. The projected population of the study area was estimated to reach 632,146 by 2017, with the majority of people living in rural areas [29]. Currently the population is above this number. Rain-fed agricultural activities, such as growing crops and raising livestock, are the primary economic activities in the watershed.

2.2. Data acquisition

2.2.1. Gauged meteorological stations data

Daily rainfall data was gathered from seven weather stations (Table 1) over an 11-year period spanning from 2009 to 2019, from the National Meteorology Agency (NMA). It was used to validate the satellite rainfall products. In this regard, Alemu and Bawoke [30]

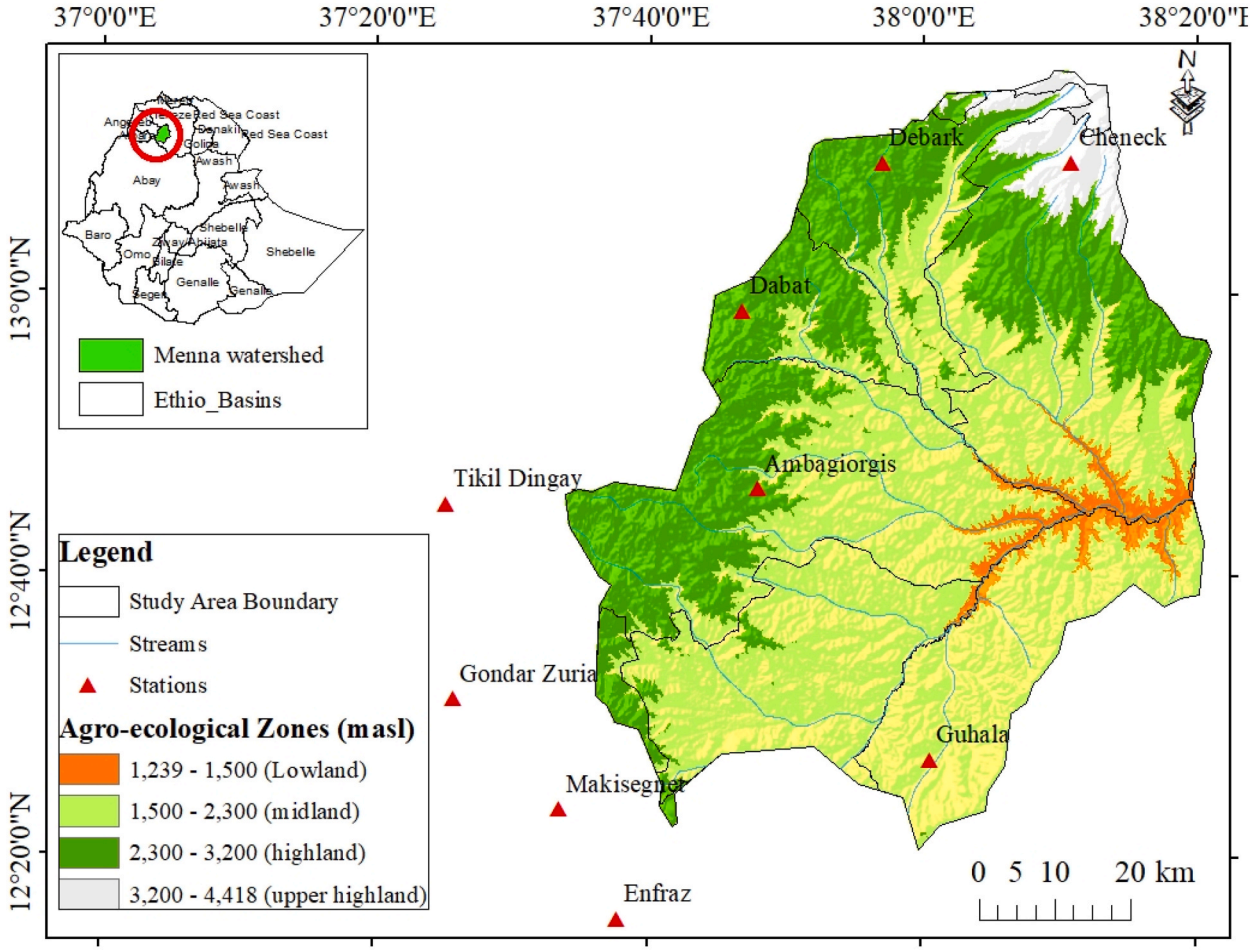

Fig. 1. Map of the study area.

carried-out satellite rainfall validation by using 11 years measured rainfall data (2000–2010) from eight independent weather stations in ANRS.

2.2.2. CHIRPS precipitation data

The main dataset used in this study was rainfall data from Climate Hazards Group Infrared Precipitation with Station data (CHIRPSv2). The Climate Hazards Group Infrared Precipitation (CHIRP) and CHIRPS are newly developed rainfall data sets created from satellite information, offering comparatively high resolution in time and space as well as near-global coverage [31]. It was produced by the US Geological Survey (USGS) in collaboration with the Climate Hazards Group at the University of California [32]. According to Funk et al. [33], the CHIRPS dataset encompasses over 35+ years (from 1981 to the present) of geostationary thermal infrared (TIR) satellite observations. It combines high-resolution satellite imagery at 5.5 km (0.05°) resolution with data from on-site weather stations to cover a spatial range from 50°S to 50°N. This process produces gridded rainfall data over time, commonly used for analyzing rainfall patterns and monitoring drought conditions. This data can be accessed at no cost from the website ftp://ftp.chg.ucsb.edu/pub/org/chg/products/CHIRPS-2.0.

Studies like Dinku et al. [31] have proved that CHIRPS has better performance in representing the rainfall over East Africa. They recommended to use CHIRPS than the other satellite products in Ethiopia since it showed high accuracy in many parts of the country [33]. Therefore, for the present study CHIRPSv2 monthly and daily rainfall products form the period 2000–2022 were used for the purpose of assessing meteorological drought and determining the trend and spatiotemporal patterns of rainfall.

2.3. Data processing techniques

2.3.1. Filling missing values of gauged stations data

To collect the rainfall data recorded at weather stations from 2009 to 2019, stations were chosen based on their extensive historical data, minimal missing data, and how well they represented the watershed. The gauging stations are sparsely distributed across different agro-ecological zones in the region, with their placement determined by altitude (Fig. 1). For instance, Chenek is located in (*Wurich*/cool and moist), Debark and Dabat stations were located in (*Dega*/cool and humid) zones, and also Guhala in Belesa classified under *Dega and Woina-Dega* agro-ecological zones. Table 1 provides the historical background of the selected stations.

Getting access to high-quality, reliable data is one of the first tasks in any hydrological or meteorological investigation [34]. Nevertheless, missing values in the data from some stations could hinder accurate statistical analysis, hydrological and environmental modeling, and monitoring of meteorological drought [35]. To prevent such issues, all of the data underwent strict data quality control by carefully checking for outliers and missing values. As a result, some of the input data obtained were totally or partly missing, which may be due to instrument failures, recording or reporting errors [36]. To obtain continuous data, missing records were completed using the mean method (replaced with the mean) and the Normal Ratio method (NR) when the percentage of missing values was below 10% [37]. Finally, XLSTAT version 2021 was used for applying the data filling techniques.

2.3.2. Validation of CHIRPS rainfall estimates

To assess and track droughts effectively, it is essential to have accurate data on rainfall at various spatial and temporal scales [38]. However, the distribution of gauging stations are sparse and uneven across Ethiopia [39]. Satellite and reanalysis precipitation products have emerged as a substitute source in recent years, offering near-global estimates of precipitation at a better spatial and temporal resolution [40]. Despite this, a majority of satellite rainfall products are liable to inaccuracies because of the nature of remote sensing data and the assumptions made in retrieval algorithms. Hence, validating and checking the data is the primary task for making the result accurate and better [41,42].

This study involved assessing the CHIRPS satellite's daily rainfall data obtained from corresponding station locations during the same time period. The evaluation was done by comparing it with ground-based rainfall data recorded at seven separate weather stations over seasonal and annual timeframes. Therefore, the evaluation employed several pair-wise comparison statistical techniques including the Pearson correlation coefficient (r), mean error (ME), mean absolute error (MAE), root mean square error (RMSE), and percent bias (PBias). Likewise, Alemu and Bawoke [30], and Wassie et al. [18] utilized these methods to assess the CHIRPS satellite rainfall data against the respective ground-based observation data in different parts of Ethiopia.

*The Pearson correlation coefficient (*r*)* is a widely-used approach for assessing linear correlation. It varies from −1 to 1 and measures

Table 1
History of the observed gauging stations in Menna watershed.

Station Name	Record Length	Class	Latitude	Longitude	Elevation	Woreda
Ambagiorgis	1992–2021	3	12.77	37.62	2508	Wogera
Cheneck	2007–2019	3	13.26	38.18	3739	Janamora
Dabat	2009–2019	4	12.98	37.75	2527	Dabat
Debark	1993–2022	1	13.15	37.89	2900	Debark
Guhala	2013–2019	3	12.24	38.05	1752	Belesa
Gondar	1952–2021	1	12.52	37.43	2064	Gondar
Enfraz	1977–2021	3	12.26	37.63	1111	Enfraz
Makisegnet	1970–2021	3	12.39	37.56	1935	Makisegnet
Tikil Dingay	2002–2020	4	12.75	37.42	2020	Sanja

the strength and direction of the association between two variables. If the value of r falls between 0 and 1, it suggests a positive correlation.no correlation when 0, and negative correlation when r is between 0 and -1 [43]. Equation (1) is applied for computing the Pearson correlation coefficient.

$$r = \frac{\sum (O - \bar{O})(S - \hat{S})}{\sqrt{\sum (O - \bar{O})^2}\sqrt{\sum (S - \hat{S})^2}} \tag{1}$$

Where, r = the correlation coefficient, O = observed rainfall, $\bar{O}$ = average observed rainfall, S = satellite rainfall, $\hat{S}$ = average satellite rainfall.

The Mean Error (ME) represents the mean of errors within a collection of measurements. When comparing CHIRPS rainfall and observed rainfall, a ME value that is positive signifies an overestimation of the CHIRPS rainfall, while a negative value suggests an underestimation. A ME value of zero reflects a perfect score or absence of error. Equation (2) is utilized for calculating ME.

$$ME = \frac{\sum (S - O)}{n} \tag{2}$$

Where, ME = mean error, S = satellite rainfall, O = observed rainfall, and n = number of data points.

The Mean Absolute Error (MAE) is a metric used to evaluate errors between corresponding observations (CHIRPS rainfall data and station-based rainfall) regarding a specific matter. It is the mean of the absolute errors between data points. MAE values range from 0 to positive infinity, with an approach to zero indicating minimal error between the two sets of measurements. The calculation of MAE can be carried out using the equation provided below (Eq. (3)):

$$MAE = \frac{\sum |S - O|}{n} \tag{3}$$

Where, MAE = mean absolute error, S = satellite rainfall, O = observed rainfall, and n = number of data points.

The Root Mean Square Error (RMSE) is utilized to assess the average magnitude of the estimated errors between CHIRPS satellite rainfall data and station rainfall (Eq. (4)). A decrease in RMSE values suggests stronger central tendencies and less extreme errors between the variables. A RMSE value of zero signifies a perfect score.

$$RMSE = \sqrt{\frac{\sum_{i=1}^{n} (Si - Oi)^2}{n}} \tag{4}$$

Where, RMSE = root mean square error, *Oi* = observed rainfall, *Si* = satellite rainfall, and n = number of data points.

Conversely, the Bias indicates the degree of similarity between the mean rainfall measured by satellite and the mean of observed rainfall. A bias value near one implies a closer match between the average satellite rainfall estimation and the total observed rainfall. The bias ratio serves as an error indicator for the systematic error component, with a perfect score of 1. Deviations from this value, whether below or above 1, suggest underestimation or overestimation, respectively (Eq. (5)).

$$PBias\ (\%) = \frac{\sum (\hat{S} - \bar{O})}{\sum \bar{O}} * 100 \tag{5}$$

Where, PBias is the Percent of bias, $\hat{S}$ is mean of the satellite estimates, and $\bar{O}$ is mean of the observed rainfall.

2.4. Data analysis

2.4.1. Rainfall trend and variability analysis

2.4.1.1. Mann-Kendall's trend test. Analyzing rainfall patterns is crucial for countries such as Ethiopia, where food security and economic stability rely heavily on the timely precipitation availability [23]. Various techniques have been developed in recent years to analyze rainfall trends, such as the Mann-Kendall (MK) test, Sen's slope estimator, Spearman's rho test, cumulative sum, and linear regression [44,45]. Among these, the Mann-Kendall trend test is the most frequently utilized method [46] to identify statistically significant or insignificant trends in hydro-meteorological factors [47]. The MK test is a robust tool for identifying consistent upward or downward trends in climate parameters on a yearly or seasonal basis, and is less influenced by outliers [48,49].

In the present study, therefore, MK test was employed to examine the trend of rainfall pattern using monthly data series of 23 years (2000–2022). The test's null hypothesis (H0) asserts that the data exhibit no trend and are both independent and identically distributed; while the alternative hypothesis (H1) suggests that there is a trend present in the series, either increasing or decreasing. It uses two types of statistics based on the number of data values: S-statistics is utilized when there are fewer than 10 data values, and Z-statistics is used for data values equal to or greater than 10. In addition, every data point is also compared with every other data point. The S statistic increases by 1 when a data value from a later period is higher than a data value from an earlier period, and decreases by 1 when the earlier sampled data value is greater than the later one. The final value of S is obtained by averaging all such changes [50].

Equation (6) provides the value of the test statistic S.

$$S = \sum_{i=1}^{n-1} \sum_{j=i+1}^{n} \mathrm{sgn}(\mathrm{xj} - \mathrm{xi}); with\ sgn(xj - xi) = \begin{Bmatrix} +1, if(xj - xi) > 0 \\ 0, if\ (xj - xi) = 0 \\ -1, if(xj - xi) < 0 \end{Bmatrix} \quad (6)$$

The application of trend test is done to a time series Xi that is ranked from i = 1,2 … n-1 and Xj, ranked from j = i+1,2 … n. Each data point Xi is selected as a reference point and then compared with the remaining data points Xj. The sign function sgn(xj−xi) is calculated, with Xi and Xj representing the annual values in years i and j (where j is greater than i), respectively. After considering all the variations, this statistic represents this statistic represents the number of positive differences less the number of negative differences.

The a positive or negative value of S indicates an upward (increasing) or downward (decreasing) trends, respectively [50]. A positive or negative S value indicates an upward or downward trend, respectively. When the dataset includes 10 or more values, the S-statistics follow an approximately normal distribution. The test is carried out using a normal distribution with the mean and variance specified in equation (7).

$$\mathrm{V(S)} = \frac{\mathrm{n(n\ -\ 1)(2n + 5)} - \sum_{i=1}^{n} ti(i-1)(2i+5)}{18} \quad (7)$$

Where, n is the number of observation and ti are the ties of the sample time series. The standard normal distribution (Z–statistics) is computed using equation (8):

$$\mathrm{Z} = \begin{cases} \dfrac{5-1}{\sqrt{var(S)}}, S < 0 \\ 0, S = 0 \\ \dfrac{5+1}{\sqrt{var(S)}}, S < 0 \end{cases} \quad (8)$$

In the MK test statistics, Z conforms to the standard normal distribution with a mean of zero and a variance of one. Therefore, a positive or negative Z value signifies an upward or downward trend, respectively.

Once the presence of a trend has been determined, the strength of the trend was quantified using Sen's slope test, which is viewed as a median for all data sets across different combinations. Finally, four different alpha (α) levels at 0.001, 0.01, 0.05, or 0.1 are used to check its significance. XLSTAT 2021 was used to identify trends, fix the magnitude and check its significance level.

2.4.1.2. Coefficient of variation. The coefficient of variation (CV) was utilized to assess the variation in rainfall on an annual and seasonal basis. As discussed in Achite et al. [51], CV is a statistical measure expressed as a percentage that indicates the degree of variability of data points in a data set relative to the mean. A larger CV value indicates that the rainfall time-series data is more variable, and the climate will be less predictable. It was computed using equation (9).

$$CV = \frac{\sigma}{\bar{x}} * 100 \quad (9)$$

Where, σ is the standard deviation and $\bar{x}$ is the average rainfall. Typically, CV values were categorized as follows: low variability (CV < 20%), moderate variability (20% < CV < 30%), high variability (CV > 30%), and very high variability (CV > 40%) [52].

2.4.2. Determining the onset, cessation, and length of rainy seasons

Alterations in the timing of seasonal cycles of rainfall and shifts in the start and end of precipitation play a crucial role in agricultural operations [53]. Hence, plant water availability is highly dependent on the timing (onset, cessation & length) of rainy seasons. It subtly conveys information about the climate suitability for crop production and the likelihood of success or failure during a given season [54]. To study the start, end, and duration of rainy seasons, the average daily rainfall (Ei) for each day of the year from January 1st to December 31st, the average daily rainfall ($\bar{E}$), and the cumulative daily rainfall anomaly on a specific day (C(d)) were computed using the Climate Data Tool (CDT) platform integrated the R software [55]. The equation below (Eq. (10)) is used for the analysis.

$$C(d) = \sum_{i=1jan}^{d} \mathrm{E} - \bar{\mathrm{E}} \quad (10)$$

2.4.3. Meteorological drought assessment

2.4.3.1. Percent of normal (PN). According to Gibbs and Maher [56], the percent of normal can be calculated on various time scales such as daily, weekly, monthly, seasonal, and yearly, catering to the diverse requirements of users. It is very easy to calculate with basic mathematics, regularly generated by various climate software packages, and easy to understand by the media and the public. PN can be utilized to compare different time intervals in any specific area. It is determined by dividing the actual precipitation by the average

precipitation, and then multiplying the outcome by 100 for the period under consideration (Eq. (11)).

$$PN\ (\%) = \frac{Ri}{\hat{R}} * 100 \tag{11}$$

Where, PN = percent of normal, Ri = actual rainfall, $\hat{R}$ = long-term mean rainfall.

The percent of normal precipitation can be applied to detect and track different effects of droughts. It also categorizes droughts into five severity levels (Table 2).

2.4.3.2. Standardized anomaly index (SAI). SAI, also referred to as the rainfall deficit index, indicates the number of standard deviations by which a rainfall figure deviates from the historical average [21]. It is applicable for identifying drought events, especially in areas frequented by droughts. SAI can be computed over any specified time frame, but it solely relies on precipitation data, and the accuracy of calculations hinges on the quality of the data available [58]. The equation below (Eq. (12)) summarizes the competition procedures of SAI, and the classification for the drought severity levels is indicated in Table 3.

$$\mathrm{SAI} = \frac{\mathrm{Ri} - \hat{R}}{\sigma} \tag{12}$$

Where, Ri = actual rainfall, $\hat{R}$ = long-term mean rainfall, and σ = the standard deviation.

Several studies [17,18,20,59] have used SPI instead of SAI or interchangeably to characterized meteorological droughts in Northeastern highlands of Ethiopia. However, the present study applied SAI mainly to show the spatial distribution of meteorological drought in the area. Meanwhile, 176 grid points were extracted from CHIRPS data set, and then interpolate it by using ordinary Kriging interpolation techniques to get continuous features for the study area.

2.4.3.3. Standardized precipitation index (SPI). SPI is a powerful recommended tool in detecting drought incidences and characterizing its effect [58]. SPI has a number of advantages as compared with other meteorological indices. Firstly, the evaluation of SAI is straightforward as it is solely dependent on precipitation data. Second, it can detect and characterize droughts on multiple time scales. Thirdly, the standardization SPI makes it well suited to compare droughts across different time periods and regions with varying climatic condition [56,58].

Different from SAI, SPI was calculated by applying a gamma distribution function to a frequency distribution of precipitation amounts during a defined timeframe at a particular location [60]. The SPI calculation for any given location relies on the historical precipitation data over a specific timeframe. In order to maintain a mean SPI of zero for the specified time and location (with half of the precipitation totals falling below the median and half above it), the long-term precipitation data is adjusted to a probability distribution and then transformed into a normal distribution [61]. In essence, the alpha (α) and beta (β) values of the gamma probability density function were calculated [60]. This allowed for the approximate conversion of the cumulative probability distribution function into a standard normal cumulative distribution with a mean of zero and a standard deviation of one. Meanwhile, the probability of observed precipitation is converted into an index [17].

The gamma conversion involved applying the *t*-transformation, and SPI was subsequently computed based on the values resulting from the gamma transformation: $c0 = 2.5155517$, $c1 = 0.802853$, $c2 = 0.010328$, $d1 = 1.432788$, $d2 = 0.189269$, and $d3 = 0.001308$ [60]. Hence, the following equations (Eq. 13, 14, 15, 16) are applied subsequently.

$$Commulative\ Gamma\ Transformation = G\ (x, \alpha, \beta) = \frac{1}{\alpha^{\beta}\Gamma\beta}\int_0^x x^{\beta-1}e^{-x/\alpha}dx \tag{13}$$

$$Gamma\ function = \Gamma\beta = \int_0^x x^{\beta-1}e^{-x}dx \tag{14}$$

The maximum likelihood is used to estimate α and β thus:

$$\text{Shape parameter } (\alpha) = \frac{1}{4\mathrm{U}}\left[1 + \sqrt{1 + \left(\frac{4U}{3}\right)}\right] \tag{15}$$

Table 2
Percent of normal precipitation drought category.

PN VALUE (%)	DROUGHT CATEGORY
≥ 120	Humid
80–120	Normal/no drought
70–80	Light/mild drought
55–70	Moderate drought
40–55	Severe drought
< 40	Extreme drought

Source [57].

Table 3
Drought categories defined for SAI/SPI indices.

SAI/SPI value	Drought category
≥ 2.0	Extremely wet
1.5 to 1.99	Very wet
1.0 to 1.49	Moderately wet
0.99 to −0.99	Near normal or Mild drought
−1.0 to −1.49	Moderate drought
−1.5 to −1.99	Severe drought
≤ −2.0	Extreme drought

Source [58].

$$Scale\ parameter(\beta) = \frac{\overline{X}}{\beta} \tag{16}$$

Where : $U = \ln(X) - \overline{X}_{ln}$; $\overline{X}_{ln} = \frac{\sum ln(X)}{N}$; $\overline{X} = \frac{\sum X}{N}$, and N = number of precipitation observations, X = annual precipitation amount

The parameters obtained (α, β and U) are utilized to calculate the cumulative probability of a recorded precipitation event within the specified year in the dataset. These parameters are applied to the gamma probability density function to determine this cumulative probability. The cumulative probability distribution is then adjusted to match the standard normal cumulative distribution, ensuring that both have the same probability [62]. Hence, the t-transform and the SPI based on it are computed based on the expressions arranged below (Eqs. (17)–(20)).

$$\mathrm{t-transform\ (t)} = \sqrt{ln\left[\frac{1}{X_g}\right]}, \text{where } X_g \leq 0.5 \tag{17}$$

$$\mathrm{or, t-transform\ (t)} = \sqrt{ln\left[\frac{1}{1-X_g}\right]}, \text{where } X_g \leq 1.0 \tag{18}$$

$$SPI = -\left[t - \frac{C_0 + C_1 t + C_2 t^2}{1 + d_1 t + d_2 t^2 + d_3 t^3}\right], where\ X_g \leq 0.5 \tag{19}$$

$$or, SPI = +\left[t - \frac{C_0 + C_1 t + C_2 t^2}{1 + d_1 t + d_2 t^2 + d_3 t^3}\right], where\ X_g \leq 1.0 \tag{20}$$

Since a precipitation distribution could include values of zero and the gamma function is not defined at x = 0, the resulting cumulative probability is (Eq. (21)):

$$H(x) = q + (1-q)G(x) \tag{21}$$

Where, q is the probability of a zero. Next, to obtain SPI, the cumulative probability H(x) is converted to the standard normal distribution [63]. The entire process that was employed to determine the SPI is detailed in Ref. [60].

However, due to the complexity of following these steps to compute SPI manually, the SPI values at four time-scales (SPI-1, SPI-4, SPI-6 and SPI-12) were calculated using R software packages. Here, SPI-1 is for July (month of maximum rainfall), SPI-4 covers June, July, August and September, SPI-6 covers the period of April–September, and SPI-12 covers September–August. SPI-1 and SPI-4 represent short-term drought conditions in the region, while the six-month SPI signifies medium-term drought and the twelve-month SPI signifies long-term drought in the area. The SPI-4 was used to assess droughts of the *Kiremt* seasons denote longer rain seasons, and SPI-12 was used to assess the annual drought for the periods 2000–2022. Consequently, higher than mean rainfall was indicated by positive SPI values, and lower than mean rainfall was represented by negative values.

2.5. Classification of drought risk area

The ultimate drought risk map was produced by utilizing 23 distinct meteorological drought frequency maps based on SAI across the entire study region. Each year's binary image was transformed into a Boolean image to depict all levels of drought severity. Next, the images from each year were added together to calculate the frequency of drought at a pixel level. As Gonfa [64] has outlined and as recently applied by Wassie et al. [18], areas can be categorized as high, moderate, or low-risk zones based on the probability of drought occurrence in over 50%, 30–50%, or less than 30% of the years, respectively. Consequently, five drought risk levels were identified using this criterion to classify the frequency map: 0–1 for no drought risk; 2–6 low risk; 7–11 moderate risk; 12–16 high; and 17 and above for very high drought risk zones. Techniques similar to these were described in many studies [18–20,65] and utilized to generate maps indicating areas of meteorological drought risks across various regions of Ethiopia.

The schematic diagram of all the methods showing all the data set used and the whole analysis techniques is represented on Fig. 2.

3. Results

3.1. Validation of CHIRPS rainfall data

In this study, the validation of CHIRPS rainfall products from 2009 to 2019 was conducted by comparing them with measured rainfall data from seven different weather stations on both seasonal and annual timeframes. The CHIRPS rainfall estimates from each station points were extracted and compared with the corresponding ground observed values using statistical measures including the Pearson correlation coefficient (r), coefficient of determination (R^2), mean error (ME), mean absolute error (MAE), root mean square error (RMSE), and percent of bias (PB).

As shown in Table 4, a high correlation was observed between CHIRPS and measured rainfall at all the weather stations. At the annual level, the correlation coefficient ranged from 0.75 at Makisegnet to 0.88 at Gondar, which is relatively good. Comparatively, the lowest (0.69) and highest (0.97) correlation was registered on Makisegnet station during the *bega* season. So, the annual correlation is found to be lower than the correlation of each season. According to Dinku et al. [31], the weaker correlation between annual CHIRPS estimates at stations and actual data can be attributed to two main factors: (1) CHIRPS tends to overestimate smaller amounts of rainfall during warmer seasons due to sub-cloud evaporation, and (2) it underestimates larger amounts of rainfall during the rainy seasons because of significant cloud cover, which hinders satellite algorithms from accurately detecting precipitation. These discrepancies significantly impact the total annual rainfall measurements. In addition, the results indicated that the coefficient of determination (R^2) value ranges from 0.57 to 0.78 in the annual and from 0.48 to 0.94 in the seasonal time scales indicating a good agreement between stations' rainfall and CHIRPS satellite data.

The Mean Error for both the annual and seasonal time scales was found to be equal. Seasonally, a full negative value of ME was registered in three stations, with the highest at Enfraz (−195 mm) and the lowest at Gondar (−1.9 mm) during summer season (Table 4). Extra precipitation was recorded at the other four stations, with the greatest amount at Tikil Dingay (76.3 mm) during the *belg* season. Based on the results, an overestimation of CHIRPS is indicated by the positive value, whereas a negative value specifies underestimation relative to the observed rainfall [39]. Moreover, the Mean Absolute Error was calculated to illustrate the variation in rainfall values between different stations. Hence, the MAE value of CHIRPS from observed measurements reached 207.9 mm for seasonal and 208.5 mm for annual time scales. The comparisons of RMSE at annual and seasonal time scales again showed differences in error values between stations. Seasonally, higher RMSE are shown from Enfraz (301.1 mm) and Ambagiorgis (259 mm) stations

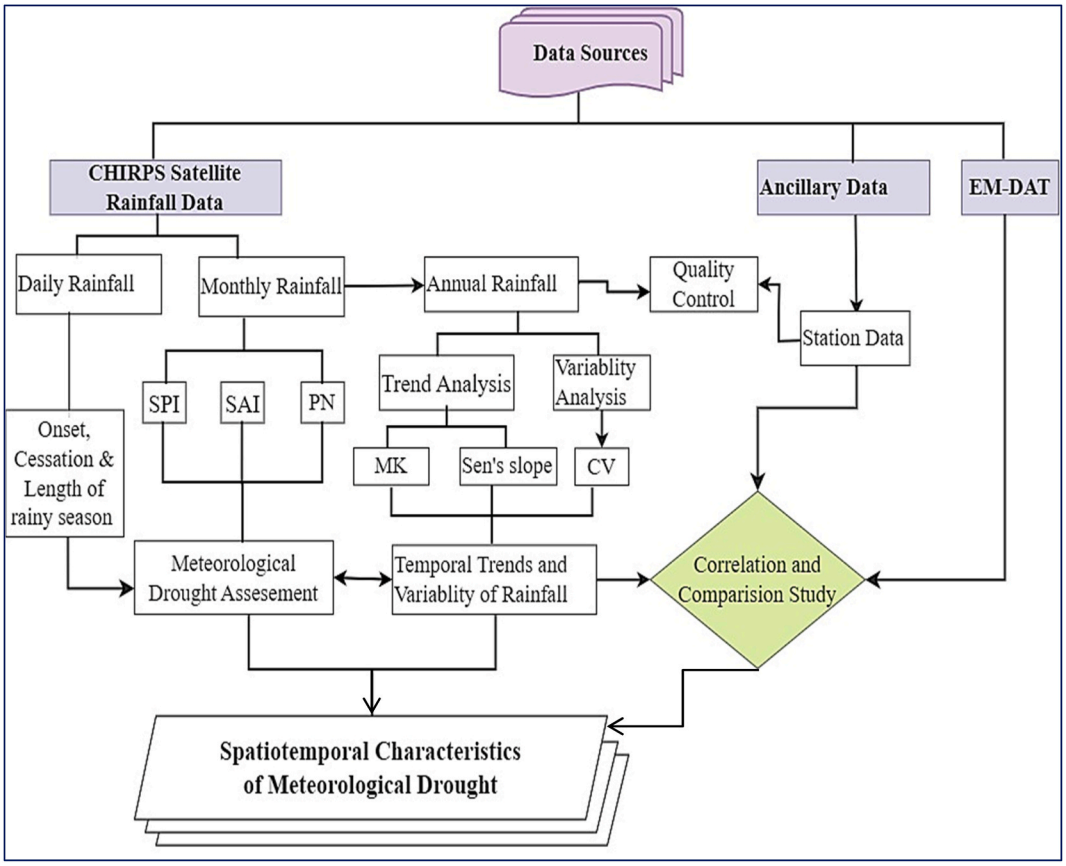

Fig. 2. Methodological framework.

Table 4
Statistical results for performance evaluation of CHIRPS rainfall.

Stations	*Seasons*	*ME*	*MAE*	*RMSE*	*r*	R^2	*PBias*
Ambagiorgis	*Annual*	−43	171.9	234.6	0.77	0.6	−4.1
	Summer	−16.4	189.2	259.0	0.79	0.62	−2.1
	Bega	−9.3	45.3	89.7	0.75	0.56	10.2
	Belg	−5.5	37.4	53.7	0.78	0.49	−3.6
Dabat	*Annual*	23.7	138.6	201.8	0.76	0.58	2.6
	Summer	4.4	62.7	82	0.84	0.7	0.6
	Bega	−25.7	50.4	113.8	0.82	0.67	−25.2
	Belg	31.8	46.8	53.5	0.78	0.6	30.2
Enfraz	*Annual*	−183.8	208.5	312.8	0.81	0.65	−14.8
	Summer	−195.5	207.9	301.1	0.8	0.64	−18.3
	Bega	−2.4	23.0	31.8	0.93	0.86	−3.4
	Belg	16.3	42.0	55.7	0.77	0.6	16.4
Gondar	*Annual*	23.6	56.5	63.8	0.88	0.78	2.1
	Summer	−1.9	62.9	75.5	0.75	0.56	−0.2
	Bega	−4.4	21.3	23.9	0.8	0.64	−4.3
	Belg	30.0	37.4	43.3	0.9	0.81	19.7
Makisegnet	*Annual*	−141.5	141.5	155.6	0.75	0.57	−13.3
	Summer	−114.1	114.1	132.2	0.69	0.48	−13
	Bega	−15.1	20.6	26.4	0.76	0.58	−21.3
	Belg	−12.3	20.8	23.4	0.97	0.94	−10.6
Debark	*Annual*	−47.8	115.3	145.2	0.81	0.66	−4.1
	Summer	−35.3	118.2	159.5	0.75	0.57	−3.8
	Bega	−5.9	24.7	32.9	0.85	0.72	−6.7
	Belg	−6.5	26.2	30.7	0.89	0.79	−3.9
Tikil Dingay	*Annual*	131	153.3	173.5	0.87	0.75	12.3
	Summer	20.0	82.3	97.3	0.8	0.64	2.3
	Bega	34.1	40.0	50.3	0.74	0.55	49.8
	Belg	76.3	76.3	81.9	0.91	0.83	71.8

during the *kiremt* season. Similarly, higher annual RMSE values are recorded in these stations. The mean RMSE for all stations was 86.6 mm for seasonal analysis and 183.9 mm for annual. This suggests that Gondar station had both a higher central tendency and lower extreme errors, with seasonal RMSE values of 23.9 mm and annual RMSE values of 63.8 mm.

Percent bias (PBias) was computed at seasonal and annual time series. Seasonally, it ranges from −0.25 in Dabat during *bega* season to 0.718 at Tikil Dingay station during *belg* seasons. Similarly, in annual scale, the PBias ranges from (−0.14) at Enfraz station to (0.12) in Tikil Dingay. Generally speaking, the bias values for most stations were below one (Table 4). This demonstrates that underestimation of rainfall (bias value < 100%) was detected in almost all stations. Likewise, the results of Alemu and Bawoke [30] in the Amhara region indicated that the CHIRPS products tended to overestimate low rainfall amounts and underestimate high values.

A scatter plot was also prepared by aggregating every data points of CHIRPS and observed rainfall in all selected gauging stations. As depicted from Fig. 3(a–g), the scatter plot was produced for each selected stations. The CHIRPS data and observed rainfall data exhibited limited variation in most stations, with a concentration of data points close to the 45° line with coefficient of determination (R^2) values between 0.8907 and 0.9303. Such higher R^2 values confirmed an acceptable agreement between the two datasets. In the area, only Tikil Dingay ($R^2 = 0.8743$), and Ambagiorgis ($R^2 = 0.7426$) stations have relatively indicated the lowest values and more scattered distribution of the data points. As concluded by Dinku et al. [31], the minor differences observed in the (R^2) values among the stations was because CHIRPS commonly showed variation in performances (overestimate or underestimate rainfall) with climate, topography and seasonal rainfall pattern differences.

Another scatter plot was also produced for the entire study area by taking the average values of both the CHIRPS and observed rainfall of all the station points (Fig. 3-h). Likewise, the CHIRPS data and observed rainfall data show minimal dispersion, with a clustering of data points near the 45° line and an R^2 value of 0.8846. However, there are a few data points that are more widely spread, possibly due to uncertainties in station locations, or systematic or random errors in ground-based rain measurements or satellite records. Therefore, it is to mean that 88.5% of the time, a 1 mm increase in CHIRPS rainfall in each month was accompanied by a 0.8812 mm rise of observed rainfall over the entire study area; a minimum difference. Furthermore, the high coefficient of determination (R^2) value of 0.8846 indicates a strong statistical correlation, demonstrating the close agreement between the observed rainfall and CHIRPS rainfall data. This result aligns with previous studies conducted by Wassie et al. [18] in North Wollo, Geleta and Deressa [66], and Bayissa et al. [67] at the watershed level in Ethiopia, where R^2 values of 0.82, 0.84, and 0.86 were reported, respectively.

Generally, all the validation result revealed that CHIRPS rainfall datasets could potentially be effective in detecting and assessing drought conditions, specifically in less-accessible data source regions of Ethiopia in general and the study area in particular.

3.2. Spatiotemporal distribution and trend analysis of CHIRPS rainfall

Examining the spatiotemporal patterns of rainfall and identifying trends is crucial for maintaining agricultural production, managing droughts and floods, ensuring sustainable water resource management, and promoting healthy ecosystem functions [68]. As it is

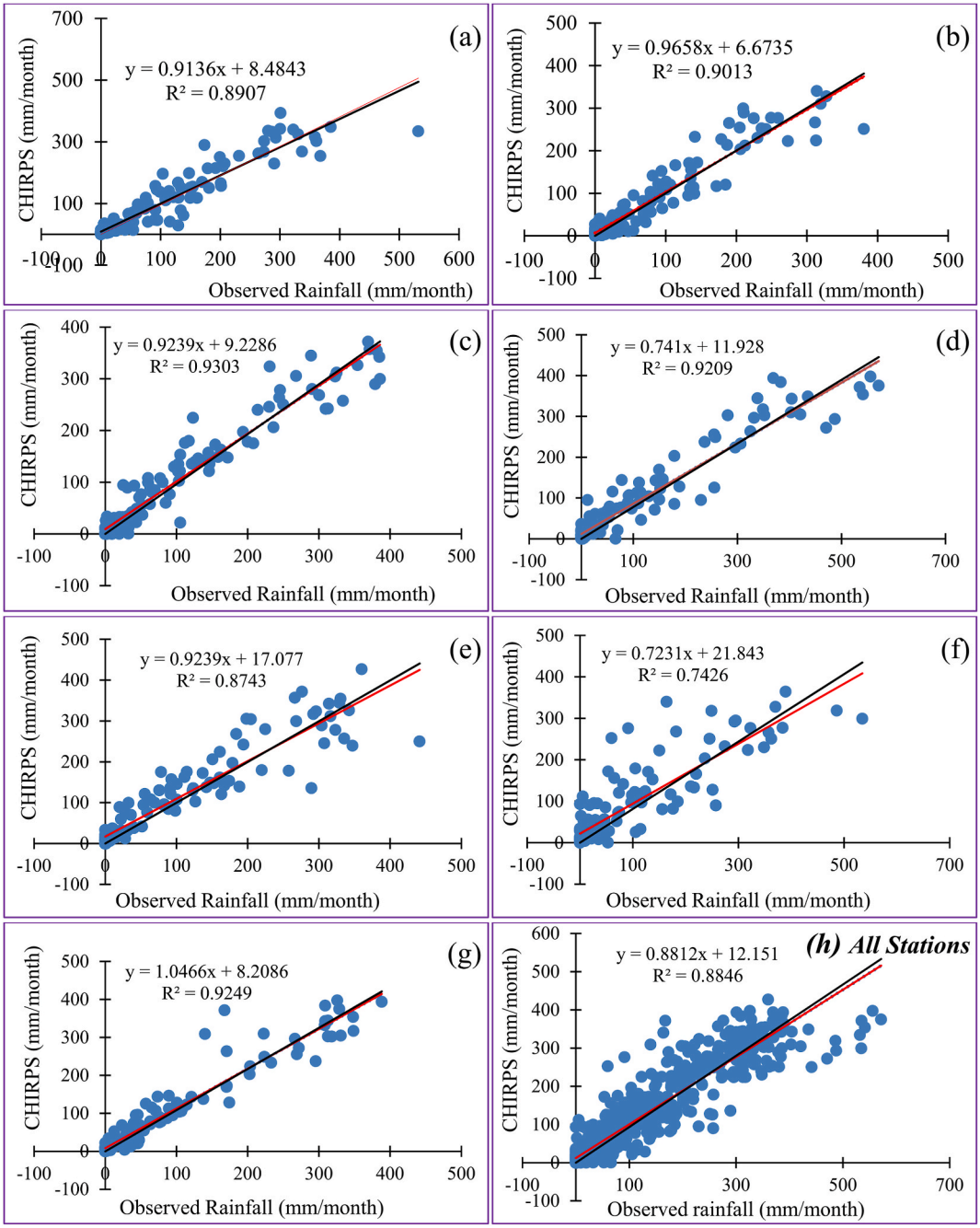

Fig. 3. Scatter plots for CHIRPS and observed rainfall selected stations at a monthly time-scale (2000–2022). In the figure, Debark station is represented (a), Dabat (b), Gondar (c), Enfraz (d), Tikil Dngay (e), Ambagiorgis (f), and Makisegnet (g). The solid black line denotes a one-to-one link, while the red line depicts the linear regression fit. (For interpretation of the references to color in this figure legend, the reader is referred to the Web version of this article.)

observed from Fig. 4(a–d), the whole part of the study area receives maximum amount of rainfall during the *kiremt* season. The highest annual rainfall levels (1340 mm/year) were recorded in the highland region, while the lowest (590 mm/year) were observed in the lowland section of the study area. The spatiotemporal distribution of such rainfall plays a great role in monitoring drought phenomena in the area.

In the region, the *kiremt, bega,* and *belg* seasons have accounted for approximately 80.6%, 6.7%, and 12.7% of the total annual precipitation, respectively. Studies conducted by Wassie et al. [18] in North Wollo, Mekonen [17] in South Wollo, and Ayalew [22] in the Amhara Region reached a similar conclusion that the *kiremt* season receives the largest proportion of the total annual rainfall.

Additional studies carried out in various regions of Ethiopia, such as [18–20,65], consistently showed that the *kiremt* season contributes the highest proportion (54–85%) of the total annual precipitation, with the *belg* season accounting for approximately 5–30%, and the *bega* season making up the smallest share (4–15%).

In the entire study area, a 984.2 mm total annual rainfall has been recorded within the study period averagely in each year (Table 5). However, this amount was variable from year to year and across the different agro-ecologies. As it is observed from Fig. 5 (a, b), and Table 5 there was variation of rainfall across seasons in the time series. The maximum amount of monthly rainfall was recorded during the year 2001 (1127.1 mm), 2007 (1047.8 mm), and 2017 (1054 mm), whereas the minimum amount of rainfall was recorded in the year 2009 (777.1 mm) and 2015 (849.7 mm). Therefore, such minimum and maximum distribution of rainfall in the area reflects the wet and drought years. A study conducted by Senamaw et al. [20] in Waghmara zone (border of the study area) concluded that 2009 and 2015 were the worst drought years, while 2001, 2007 and 2017 were characterized by wet years compared to the others.

Yue and Wang [50] have highlighted the importance of trend analysis for effective water resources management, planning, and design purposes. By detecting trends in hydrological variables like discharge, runoff, and precipitation amounts, provides useful information on the future changing tendency of such variables. As previously mentioned, the *kiremt* season predominates as the main rainy season in the study area, with approximately 74.3% of rainfall occurring solely in July and August (Table 5), indicating a concentrated distribution of precipitation in the region.

The results presented in Table 5 indicate that the coefficient of variation (CV) for annual rainfall (8%) was lower compared to the CV for each season and months within the *kiremt* season. From all the seasons, *kiremt* has the lowest CV (10%). In contrast, *belg* (35%) and *bega* (33%) seasons showed the highest variation. This output is similar with Alemayehu et al. [69], who determined that *kiremt* rainfall exhibits lower variability compared to the *bega* and *belg* seasons. Similar findings were also reported by Harka et al. [23] in the Upper Wabi Shebelle River Basin in Ethiopia, demonstrating that the *belg* and *bega* seasons exhibit significantly higher rainfall variability.

The Mann-Kendall test revealed fluctuations in the consistency of rainfall trends throughout the seasons and months of the year from 2000 to 2022. The Sen's Slope estimator specified a decreasing magnitude during the August and July, which contributes to a trend of decreasing in *kiremt* rainfall. However, there was an increasing trend of rainfall in June and September (Fig. 5a). Generally, there exists a slight increase (3.4 mm/year) in total annual rainfall when averaged across all agro-ecologies of the area (Table 5, Fig. 5b). A similar output was obtained from the research conducted by Cheung et al. [70] showing a significant decline in July and

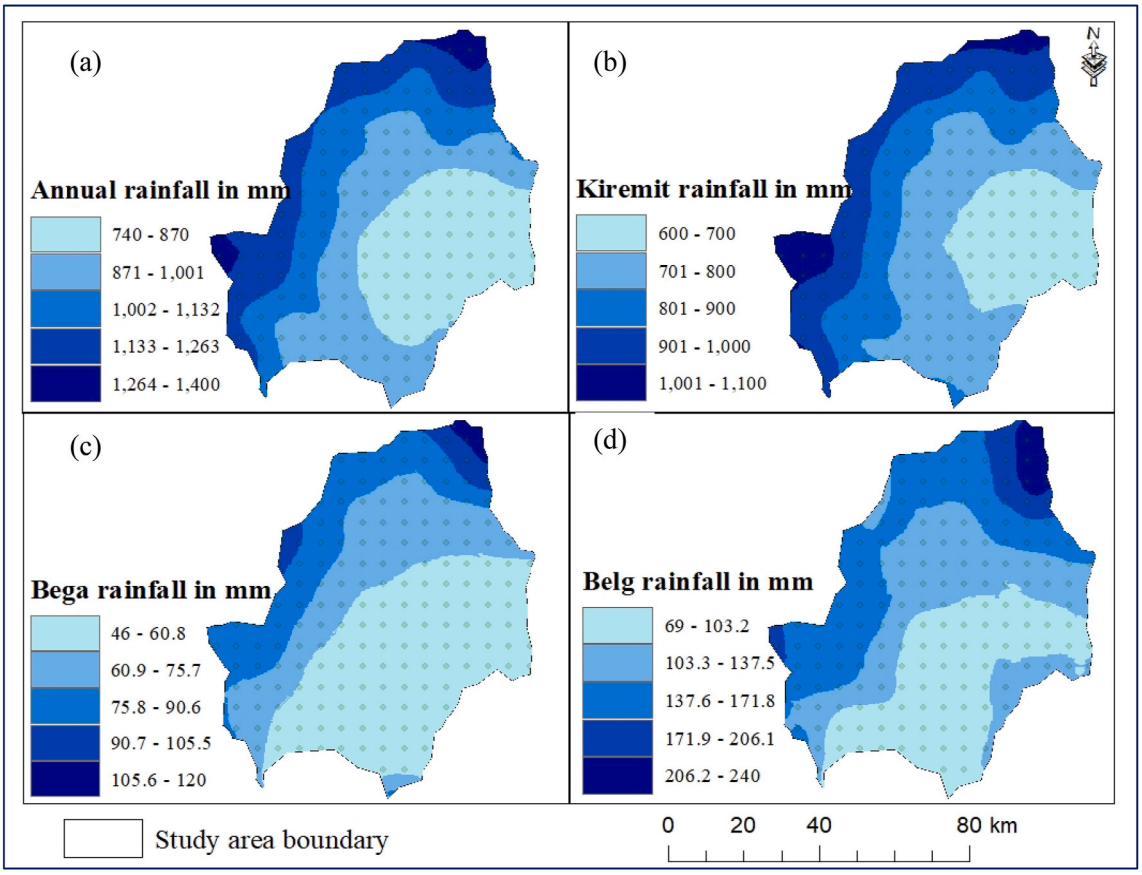

Fig. 4. The spatial distribution of rainfall in annual (a), *Kiremt* (b), *Bega* (c) and *Belg* (d) seasons in Menna watershed (2000–2022).

Table 5
Statistical value of monthly and seasonal rainfall.

Variable	*Min.*	*Max.*	Mean	%	CV%	Std. D	P value	Zs	MK	Sen's Slope
Annual	777.1	1127.1	984.2	100	8	86.8	**0.045**[a]	2.01	0.304	3.74
Kiremt	620.8	974.8	793.3	80.6	10	82.8	1.000	0.0	0.004	−0.65
Belg	62.0	253.0	125.0	12.7	35	44.7	**0.013**[a]	2.48	0.375	3.38
Bega	38.0	124.1	65.9	6.7	33	22.2	0.073	1.79	0.273	1.09
June	82.8	168.6	115.6	14.6	20	23.5	0.635	0.47	0.075	0.46
July	175.1	431.2	299.5	37.8	19	58.1	0.492	−0.68	0.107	−0.27
August	225.6	367.6	289.9	36.5	14	42.1	0.460	−0.73	−0.115	−1.80
September	45.5	143.6	88.4	11.1	23	21.2	0.369	0.89	0.138	0.97

[a] Bold value indicates statistically significant at $p < 0.05$; -Ve value indicates a decreasing trend.

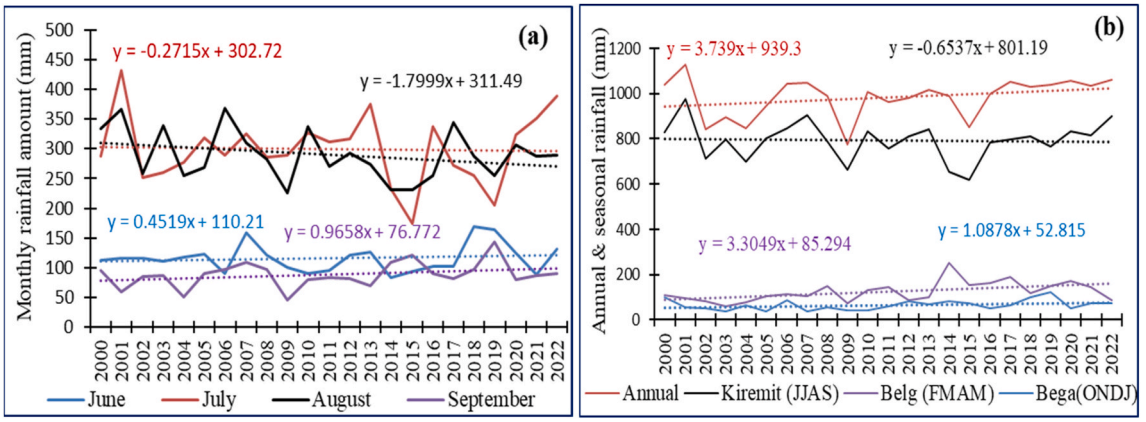

Fig. 5. Monthly (a), annual and seasonal (b) rainfall distribution of Menna watershed (2000–2022).

August rainfall over the southwestern and central parts of Ethiopia. Alemayehu et al. [69] also reported a significantly increasing trend of annual rainfall in the Alwero watershed, in western Ethiopia. Similarly, Bewket and Conway [71] reported a statistically significant increasing trend in annual rainfall in Dessie and Lalibela towns for the period 1975–2003. Conversly, these results are in opposition to the conclusions drawn by Asaminew et al. [72], Ademe et al. [73], and Wagesho et al. [16], who documented decreasing trends in annual and seasonal rainfall amounts in their specific locations in Ethiopia.

3.3. Determining the onset, cessation and length of rainy seasons

The amount of water required by plants can strongly be influenced by the rainy season's onset, cessation, length, and rainfall pattern. This, in turn, may potentially determine the sufficiency or deficiency of rainfall in a season [54]. Besides, the length of dry and wet spells can have a significant impact on the growth and productivity of crops [67]. As shown in Fig. 6, a delayed onset was recorded in 2001, 2004, and between 2015 and 2016, when the rainy season began on June 24, 25, and 27, respectively (Fig. 6a). On the contrary, the onset started early during 2008, 2011, 2014, 2017, and 2020 on the respective days of May 20, 16, 19, 16, and 20, respectively. In addition, the rainy season ended early at the beginning of September during the periods 2000–2001, 2003–2004, and 2018. It, however, took a longer time to end during 2007 by extending up to September 14 (Fig. 6b). The length of the rainy seasons in the area was variable from year to year, ranging from 67 to 112 days. Shorter lengths of rainy seasons were registered in 2003, 2004, and 2016, which waited for 70, 68, and 67 days, respectively. However, over 110 long rainy days were recorded in 2008, 2011, 2014, and 2017 (Fig. 6c) (see Fig. 7).

Generally, the observed delayed onsets and shorter duration of rainy seasons have had significant impacts on the vegetation and agricultural activities in the region. The prolonged dry periods resulting from delayed onsets have put immense stress on vegetation, leading to decreased crop yields and degradation of land. This, in turn, has exacerbated the occurrence of notable droughts in the area, affecting not only the agricultural sector but also the livelihoods of communities dependent on farming. Consistent with this, De la Poterie et al. [74] concluded that the delayed onset of the main rainy season, which normally falls within the four months (June to September), was a cause for the occurrence of droughts in various regions of Ethiopia. This underscores the importance of understanding and adapting to these spatiotemporal droughts to mitigate their adverse effects on ecosystems and human populations in Ethiopia. Efforts towards sustainable water management, improved agricultural practices, and enhancing resilience to droughts are essential to address the challenges posed by these recurrent patterns of drought [1].

The pattern of the onset, cessation, and length of the rainy seasons commonly vary depending location and timeframe. The daily CHIRPS rainfall data from eight grid points was applied to show the spatial distribution of the length of the rainy season in the area

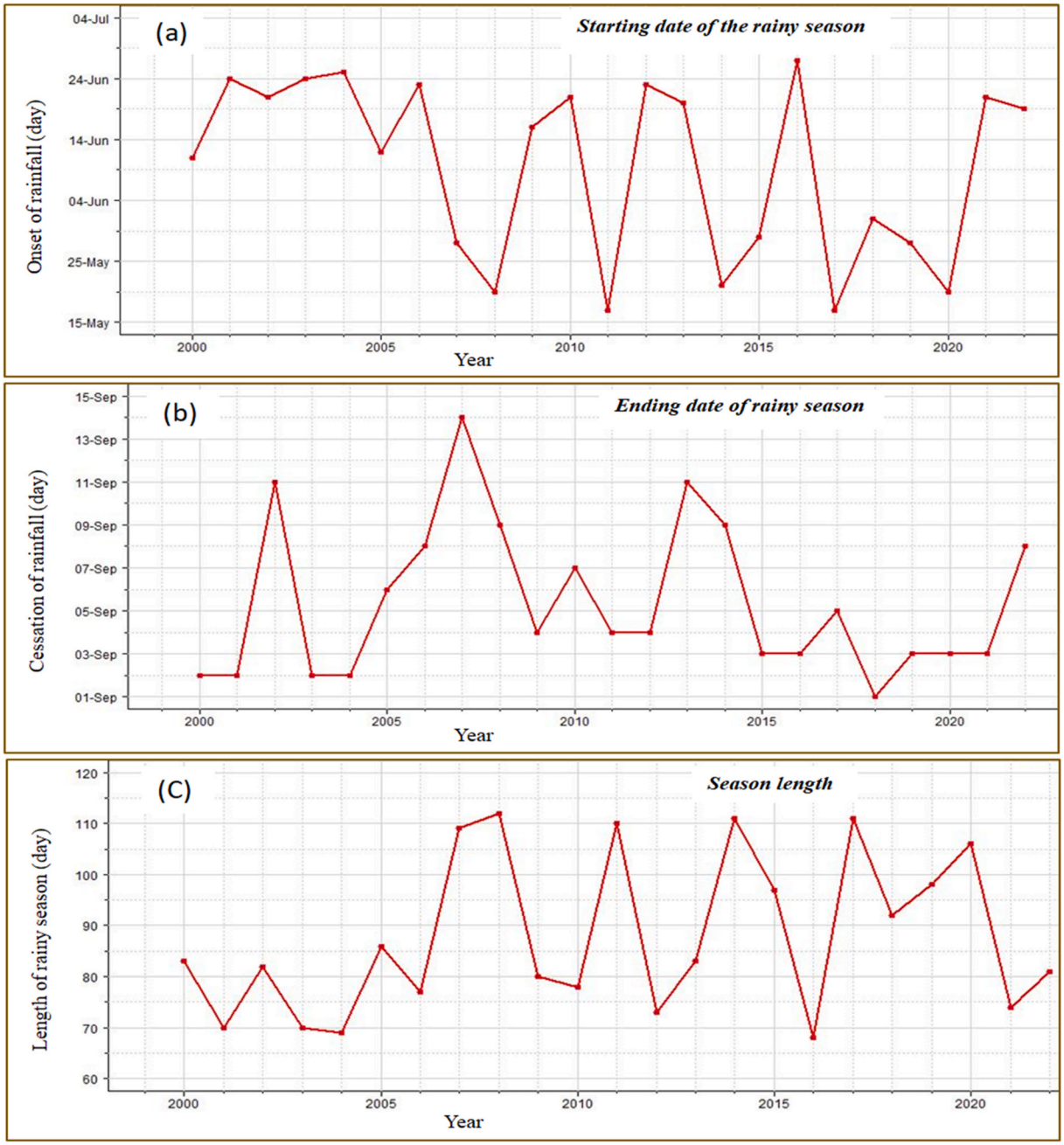

Fig. 6. The Onset (a), Cessation (b) and Length of rainy season (c) observed in Menna Watershed (2000–2022).

(Fig. 7). Accordingly, the length of rainy seasons was found to vary across the different agro-ecological zones. The highland and upper highland parts of the study area have experienced longer length of rainy seasons (over 95 days) due to the early onset and late cessation of rainfall. Conversely, lowland and midland parts of the area have experienced with a shorter length of rainy season (below 90 days). As a result, the highland and upper highland regions of the area experienced early commencement and late cessation of rainfall, contrasting the situation in the midland and lowland areas.

Fig. 8 illustrates the daily mean rainfall anomaly (blue), the accumulated daily mean rainfall anomaly (green), and the climatological daily mean rainfall for each day of the year (red) throughout the study period (2000–2022). The red dots on the Figure indicate the duration of the typical water season according to climatological data. Based on the findings, from the day of the year (365/6 days), the average day of onset was observed on the 162nd day (i.e., 6th months plus the 9th day). In other words, the onset is started on the 9th of June. Similarly, from the days of the year, the average day of cessation (ending of water season) is on the 254th day (i.e., the 9th month plus the 9th day). In other words, the cessation is started on the 9 September. The two red dots in the Figure also marked the

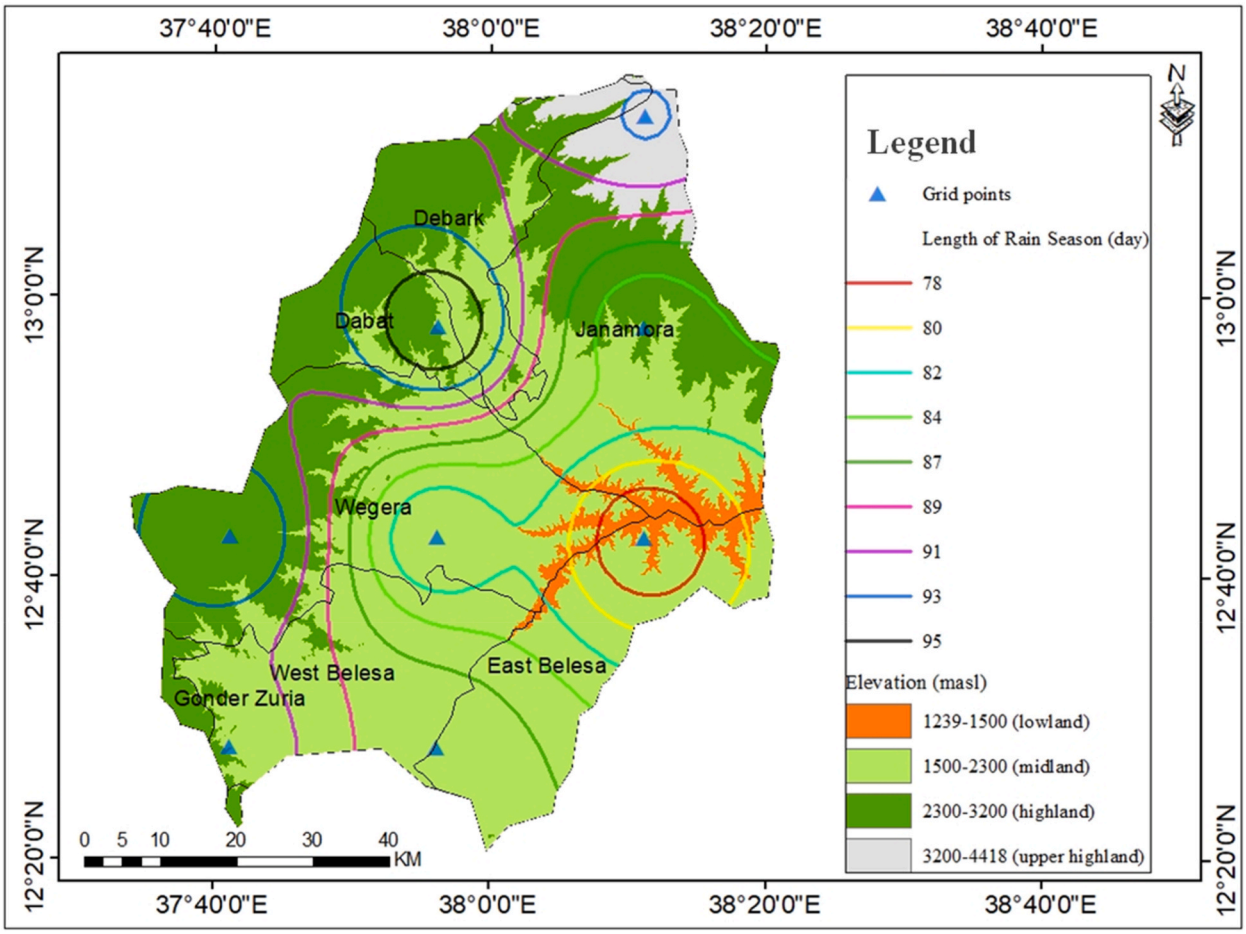

Fig. 7. Spatial distribution of the length of rainy seasons across agro-ecologies in Menna Watershed (2000–2022).

highest and lowest extent of the climatological water season of the area.

3.4. Meteorological drought monitoring using PN, SAI and SPI

To analyze the spatial and temporal distribution of meteorological drought in the study area, the percent of normal (PN),

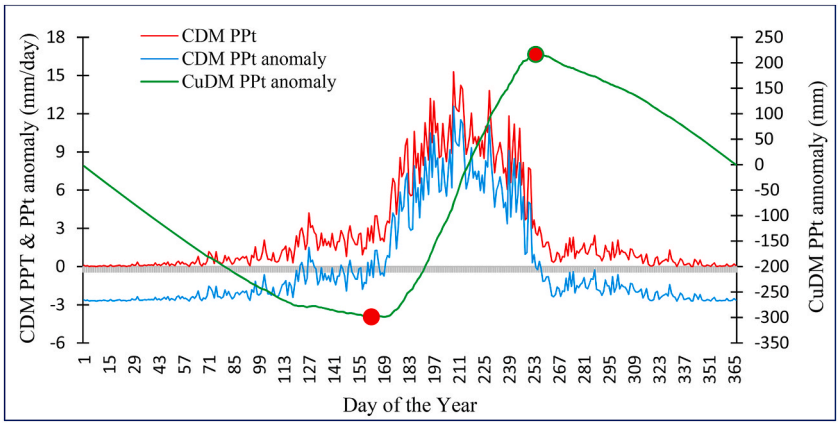

Fig. 8. Average onset and cessation of rainfall in Menna Watershed for the period 2000 to 2022
* CDM = climatological daily man; CuDM = climatological cumulative daily man; PPt = precipitation.

standardized anomaly index (SAI), and standardized precipitation index (SPI) were applied. The PN and SAI drought indices were computed in the annual (Fig. 9a), *kiremt* (Fig. 9b), *bega* (Fig. 9c), and *belg* (Fig. 9d) seasons, to observe their periodic effects. The results indicated that the PN in the annual time scale extends from the lowest 79% to the highest 114.5% in 2009 and 2001 showing mild drought and normal conditions, respectively. During the same years, the SAI value extends from −2.4 to 1.6 showing extreme drought and very wet conditions. Such computed PN and SAI values indicated that in the years 2002, 2004, 2009, 2015, and 2019, there was a distinct lack of rainfall during the main cropping season (Fig. 9b) showing drought conditions in different severity levels. The indices also revealed that excess rainfall was registered during the *bega* season in 2001, 2007, and 2020 which usually has a bad consequences for crop harvesting in the area (Fig. 9c). However, during 2014 and 2017, there have been better rainfall conditions useful for belg harvesting in the watershed (Fig. 9d). The outputs obtained from several studies in different parts of Ethiopia [17–20,75] confirmed that 2002, 2004, 2009, 2015, and 2019 were considered as drought years.

SPI is a statistical measure used to assess rainfall anomalies in a particular region over multiple time scales [60]. It quantifies the deviation of precipitation from the historical average, enabling the detection of dry periods and drought occurrences. By examining SPI values across multiple time scales, it is feasible to detect droughts occurring at different time scales, ranging from immediate to extended periods, and issue timely warnings to affected areas [56,58]. Hence, the temporal characteristics of droughts in the study area were also assessed by using the SPI values computed from the data obtained in the selected grid points (Fig. 10). Analysis of the 1, 4, 6, and 12-month SPI time series revealed the existence of droughts in different severity levels that falls between extremely wet and extreme dryness.

The SPI-1 is a one-month SPI, which provides a relatively short-term view of rainfall conditions. It assesses deviations from the average rainfall within a single month. This can help identify any sudden and significant variations in precipitation, particularly in areas like Menna watershed, where rainfall patterns are volatile. Based on the computed values of SPI-1 time scale, the extreme wet condition was registered in 2000, while 2015 was extremely dry months with SPI values of 2.06 and −2.47, respectively. On the other hand, the four-month SPI (SPI-4) encompasses a relatively longer time period, allowing for a more comprehensive analysis of rainfall patterns. It evaluates how precipitation deviates from the average rainfall over a four-month (June, July, August, and September) period. This can be useful in detecting trends or changes in rainfall for a *kiremt* season in the area for the period 2000–2022. Accordingly, based on the 4-monthly (*kiremt* season) SPI-4 value, the years 2004, 2009 and 2015 showed an extremely dry condition with the SPI scores of −2.0, −2.42 and −2.47, respectively, indicating extreme meteorological drought incidences. On the other side, extreme wet conditions were recorded in 2001, 2018 and 2019 with the SPI values of 2.06, 2.17, and 2.27, respectively.

The six-month SPI evaluates rainfall anomalies over a six-month period, providing a medium-term view of precipitation patterns. It assesses how much precipitation deviates from the average rainfall during this half-year period. This duration is effective in capturing

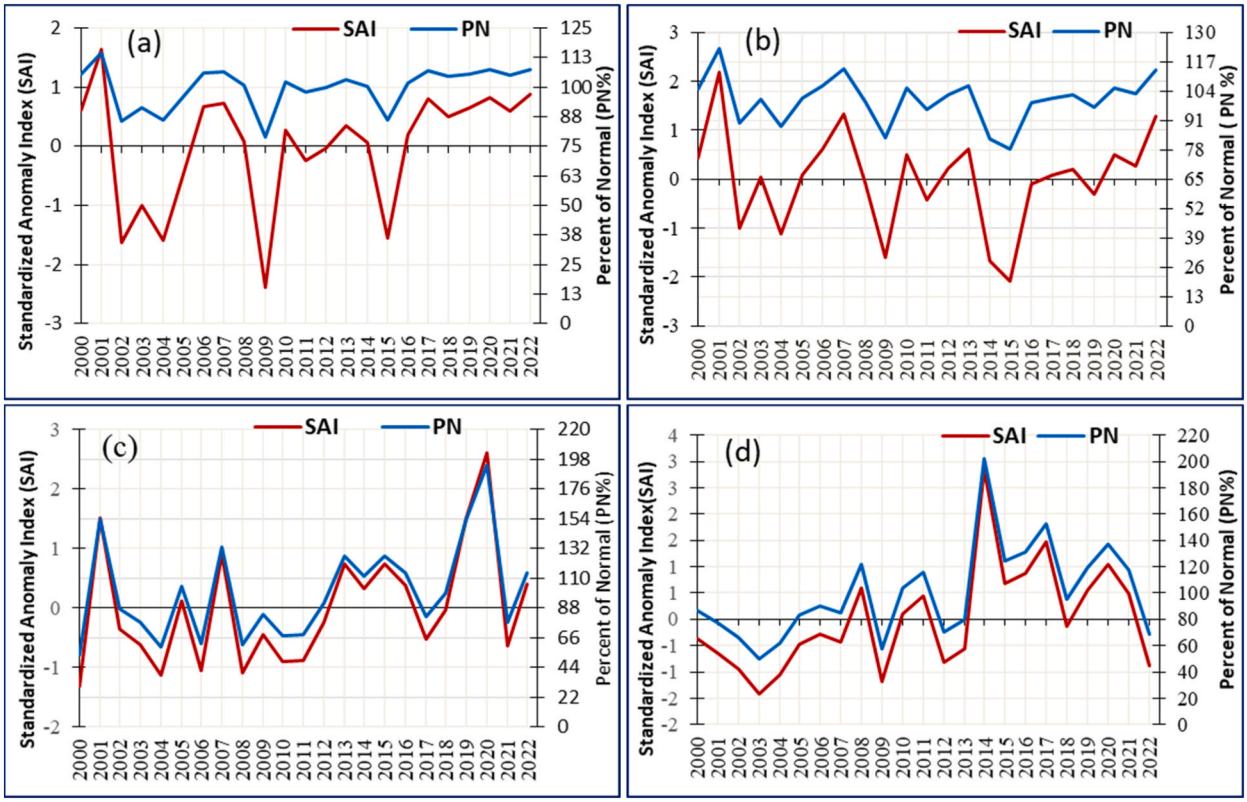

Fig. 9. Standardized anomaly index and percent of normal in annual (a), *kiremt* (b), *bega* (c), and *belg* (d) seasons.

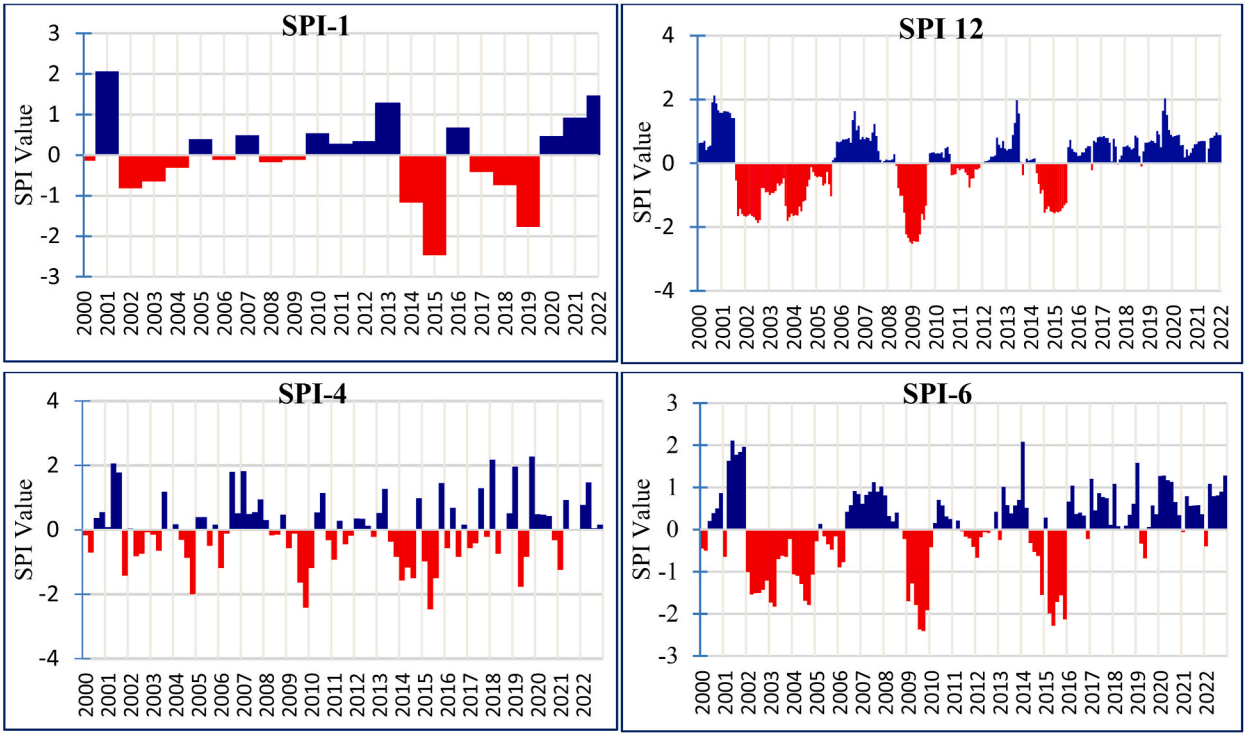

Fig. 10. Standardized precipitation index (SPI) values in Menna watershed across 2000 to 2022. The blue colors show non-drought years while the red colors show drought conditions of different severity levels. (For interpretation of the references to color in this figure legend, the reader is referred to the Web version of this article.)

seasonal variations and can be useful in identifying longer-term trends or shifts in rainfall patterns. In the SPI-6, the most extreme wet seasons were recorded in 2001 and 2014 with SPI values of 2.11 and 2.08, respectively, while its extreme dryness were registered in 2009 and 2015 with SPI values of −2.41 and −2.28, respectively.

The annual SPI (SPI-12) considers precipitation anomalies for a full calendar year. It assesses the deviation from the average annual rainfall. This longer time scale provides a comprehensive overview of annual precipitation patterns, encompassing all seasons. It helps in understanding the overall hydro-climatic conditions for a specific year and is commonly used in monitoring droughts or long-term water availability [62]. Similarly, in the SPI-12 extreme wet and dry spells were registered in 2001 and 2009 with SPI values of 2.1 and −2.4, respectively. This result basically confirmed that the years 2009 and 2015 were characterized by sever meteorological drought conditions. On the other hand, wetter conditions have been recorded under SPI-6 and SPI-12 during the periods 2000–2001, 2006–2007, 2012–2013, and 2016–2022 (Fig. 10). From these, 2001, 2010, and 2016 were relatively the wettest years.

Generally, six out of the 23 years (2002, 2004, 2009, 2014, 2015, and 2019) were characterized by a drought year. Similarly, Winkler et al. [76] based on SPI and VCI results found that the years 2002, 2004, 2009, 2010, and 2015 were extensively affected by drought events during the *kiremt* season in the area. The EM-DAT [75] disaster database also confirmed that those years are recorded as drought years in most parts of Ethiopia including the study area.

As it is observed from Fig. 11, except for some eastern lowland parts which are regularly affected by drought, the extent and severity levels of meteorological drought showed variation in time and place across the watershed. As explained earlier, 2002, 2004, 2009, 2014 and 2015 were categorized as the driest years with about 24, 27.8, 44.2, 44.6, and 56.7% of the area affected by extreme to severe drought conditions, respectively. In such drought years, only 2.7, 0.7, 1.4, 0.2, and 0.5% of the watershed was free from drought, respectively. Generally, the lowland and midland of the study area were highly affected by an extreme drought, whereas the highland and upper highland part of the watershed has been affected by mild to moderate drought. In contrast, in 2001, 2007, and 2022 about 69.3, 48.3 and 43.2% of the area were characterized by non-drought conditions. Nevertheless, the research emphasizes that there has not been a single year without drought in the region during the study period, leading to the population being consistently affected by recurring droughts.

In General, based on the result of SAI computed on rainfall of the area averaged over 23 years, more than 79% of it, mostly the lowland and midland parts, were affected by drought. From this, about 64.6% was characterized by mild drought severity level (SAI = −0.99 to 0.99) or unusually dry conditions (near normal), which slightly deviated from the regular rainfall distribution. However, such repeated lack of rainfall and drought attacks could pose a significant impact on vegetation growth.

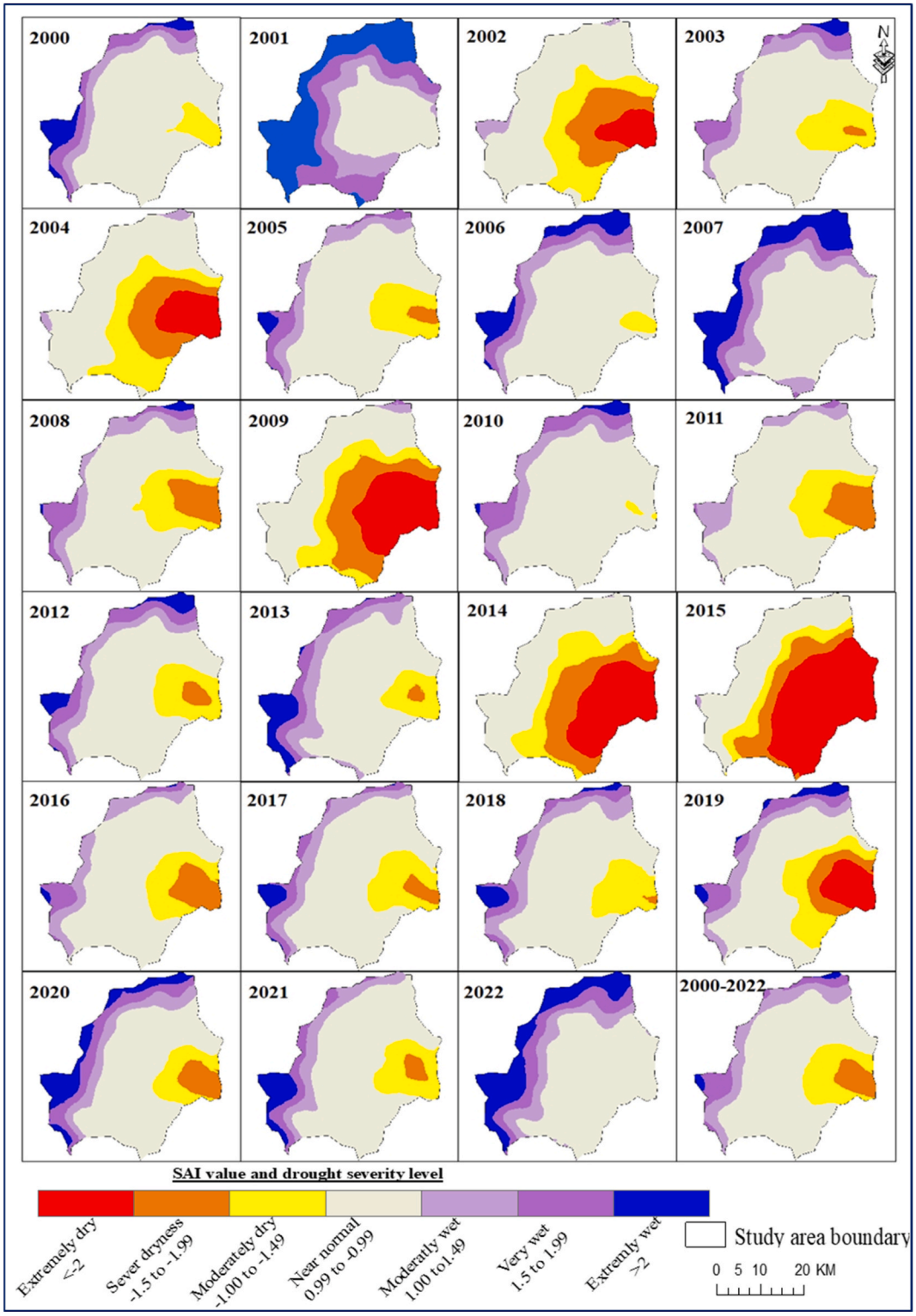

Fig. 11. Spatial and temporal distribution of meteorological drought based on SAI.

3.5. Drought frequency and classification of drought risk area

The analysis of historical drought severity maps indicates a diverse pattern of drought frequency across different locations and time periods in the study area. Specifically, the lowland region experienced more frequent occurrences of severe droughts compared to other agro-ecological zones (Fig. 12). This resulted in heightened vulnerability to short return periods of meteorological droughts in nearly all parts of the area.

The meteorological drought risk map (right bottom corner of Fig. 12) summarizes the drought conditions of the area from 2000 to 2022. In terms of area coverage, about 3.7, 8.1, 8.7, and 69.3% of the watershed were well-thought-out as low, moderate, high and very high drought risk zones, respectively. Consequently, an extremely small portion of the area (0.2%) was considered as not risky for meteorological droughts. In general, considering the frequent drought occurrence, wide coverage, and severity as shown in Fig. 12, it is possible to conclude that the whole watershed is an extremely high drought-risky area that demands continuous follow-up.

4. Conclusions and the way forward

This study assessed the trends of rainfall and spatiotemporal patterns of meteorological drought using geospatial technologies in the Menna Watershed. The analysis of rainfall patterns over time involved studying the coefficient of variation (CV), conducting the Mann-Kendall (MK) test, and applying Sen's slope estimator. In addition, the PN, SAI and SPI indices were applied to detect and characterize the spatiotemporal pattern of droughts in the area. CHIRPS rainfall estimate and station-based observed rainfall were the datasets used, where the observed rainfall was used to validate the performance of CHIRPS data set.

The pattern of rainfall in the area was highly variable in *belg* (CV = 35%) and *bega* (CV = 33%), while *kiremt* showed the lowest (10%). However, the CV for the annual rainfall (8%) was lower compared to the CV for each season and each month of the *kiremt* season. A noticeable rise in rainfall was noted annually (3.7 mm/year) and during *belg* (3.4 mm/year) at a significance level of $p < 0.05$, whereas there was a slight decrease in rainfall during the *kiremt* season (−0.7 mm/year). The onset, cessation and length of rainy

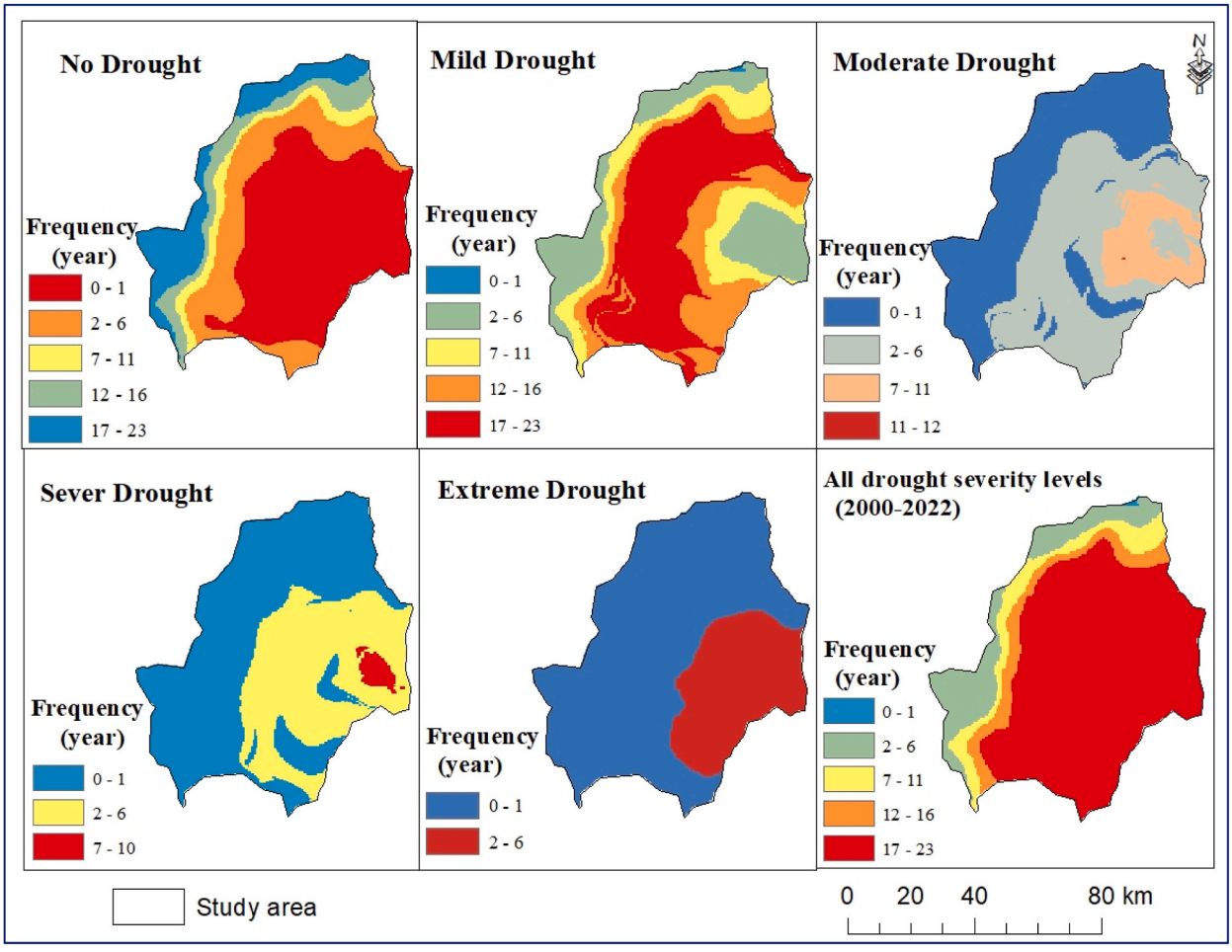

Fig. 12. Frequency (year) of meteorological drought by severity levels: extreme (**a**), sever (**b**), moderate (**c**), and slight drought (**d**).

seasons were also variable from year to year and across agro-ecologies. In the highland and upper highland regions of the area, longer rainy seasons (95–111 days) were noted with rainfall beginning earlier and ending late. Conversely, the midland and lowland areas experienced shorter rainy seasons (67–90 days). Specifically, the longer rainy seasons were recorded during 2007–2008, whereas the shorter rainy seasons were registered during 2003–2004 and 2015–2016. Such variability in rainfall patterns posed significant effects on crop production making smallholder farmers highly vulnerable to the impacts.

The PN, SAI and SPI values computed over the period 2000–2023 detected the wet and drought years. As a result, six out of the 23 years (2002, 2004, 2009, 2014, 2015, and 2019) were the detected drought years. In 2009, 2014, and 2015, severe drought and extremely dry conditions were prevalent, where only 1.4, 0.2, and 0.5% of the watershed was free from drought, respectively. In contrast, wetter conditions have been recorded during the periods 2000–2001, 2006–2007, 2012–2013, and 2016–17. Out of these years, 2001, 2010, and 2016 were identified as the wettest compared to the rest. As a result, there was spatial diversity in both the occurrence and intensity of drought events. The lowland part of the watershed has been frequently affected by severe droughts, while the highland and upper highland areas faced mild drought conditions. It is important to note that there was no year without drought in the study area, leading to the population being consistently smashed by such recurrent droughts.

The study concluded that the Menna watershed in northwestern Ethiopia is characterized by an exceptionally high risk of meteorological drought. Accordingly, about 86% of the area repeatedly encounters extreme rainfall deficit (7–23 times) leading to a high risk of meteorological droughts. Such perceived spatiotemporal meteorological drought-risk incidents pose a likely threat to the rainfed agriculture exerting an enormous effect on the livelihoods of smallholders. Therefore, the study could provide additional information to policymakers on early warning systems and regional and local drought monitoring strategies, enabling them to enhance current policies for adaptation, mitigation, and monitoring purposes aimed at lessening the effects of climate extremes and related droughts. Lastly, further study is recommended in the area by taking into account other drought indices which can help better capture and characterize meteorological droughts.

Funding information

Funding information is not applicable/No funding was received.

Availability of data

The data used during the current study will be available upon request.

CRediT authorship contribution statement

Fekadie Bazie Enyew: Writing – review & editing, Writing – original draft, Methodology. **Simachew Bantigegn Wassie:** Writing – review & editing.

Declaration of competing interest

The authors declare that they have no known competing financial interests or personal relationships that could have appeared to influence the work reported in this paper.

Acknowledgments

We have special thanks to the Climate Hazards Group at the University of California for developing the CHIRPS rainfall estimate and allowing us to freely download the data from https://data.chc.ucsb.edu/products/CHIRPS-2.0/africa_monthly/. We want thank the Ethiopian National Meteorological Service Agency for providing the time series daily rainfall data for selected stations in the study area. We are grateful for Balew Demissie (PhD), an English language expert at Addis Ababa Technology University, for giving his time in editing the manuscript with the necessary language improvement.

References

[1] G.A. Mera, Drought and its impacts in Ethiopia, Weather Clim. Extrem. 22 (2018) 24–35.
[2] D.A. Wilhite, Drought as a natural hazard: concepts and definitions, in: A. Wilhite (Ed.), Drought: A Global Assessment, Routledge, London, 2000, pp. 3–18.
[3] T. Tadesse, Strategic Framework for Drought Risk Management and Enhancing Resilience in Africa, 2016.
[4] J. Spinoni, G. Naumann, H. Carrao, P. Barbosa, J. Vogt, World drought frequency, duration, and severity for 1951-2010: world drought climatologist for 1951-2010, Int. J. Climatol. 34 (2014) 2792–2804, https://doi.org/10.1002/joc.3875.
[5] IPCC, Intergovernmental Panel on Climate Change Sixth Assessment Report (AR6): Climate Change 2022-Impacts, Adaptation and Vulnerability, Regional Factsheet Africa, 2022.
[6] UNDRR, Special Report on Drought 2021: Global Assessment Report on Disaster Risk Reduction, United Nations Office for Disaster Risk Reduction (UNDRR), Geneva, 2021.
[7] S.M. Hayes M, Drought monitoring and early warning: twenty-frst century advancements and challenges". Drought and Water Crises, Arabian J. Geosci. (2017).
[8] E. Gidey, O. Dikinya, R. Sebego, E. Segosebe, A. Zenebe, Modeling the spatio-temporal meteorological drought characteristics using the standardized precipitation index (SPI) in raya and its environs, northern Ethiopia, Earth Syst Environ 2 (2018) 281–292, https://doi.org/10.1007/s41748-018-0057-7.
[9] Z. Kalantari, C.S.S. Ferreira, S. Keesstra, G. Destouni, Nature-based solutions for flood-drought risk mitigation in vulnerable urbanizing parts of East-Africa, Current Opinion in Environmental Science & Health 5 (2018) 73–78, https://doi.org/10.1016/j.coesh.2018.06.003.

[10] T. Tadesse, G.B. Demisse, B. Zaitchik, T. Dinku, Satellite-based hybrid drought monitoring tool for prediction of vegetation condition in Eastern Africa: a case study for Ethiopia, Water Resour. Res. 50 (2014) 2176–2190.
[11] A.M. El Kenawy, M.F. McCabe, S.M. Vicente-Serrano, J.I. López-Moreno, S.M. Robaa, Cambios en la frecuencia y severidad en las sequías hidrológicas de Etiopía entre 1960 y 2013, Cuad Investig Geogr 42 (2016) 145–166.
[12] W.B. Anderson, B.F. Zaitchik, C.R. Hain, M.C. Anderson, M.T. Yilmaz, J. Mecikalski, L. Schultz, Towards an integrated soil moisture drought monitor for East Africa, Hydrol. Earth Syst. Sci. 16 (2012) 2893–2913, https://doi.org/10.5194/hess-16-2893-2012.
[13] UNOCHA, Drought in the Horn of Africa, Regional Humanitarian Overview & Call to Action, 2023. Revised 28 November 2023).
[14] E. Birara, M. Mequanent, S. Tadesse, Assessment of food security situation in Ethiopia: a review, Asian Journal of Agricultural Research 9 (2015) 55–68.
[15] Y. Bayissa, S. Maskey, T. Tadesse, S. Van Andel, S. Moges, A. Van Griensven, D. Solomatine, Comparison of the performance of six drought indices in characterizing historical drought for the upper blue nile basin, Ethiopia, Geosciences 8 (2018) 81, https://doi.org/10.3390/geosciences8030081.
[16] N. Wagesho, N.K. Goel, M.K. Jain, Temporal and spatial variability of annual and seasonal rainfall over Ethiopia, Hydrol. Sci. J. 58 (2013) 354–373, https://doi.org/10.1080/02626667.2012.754543.
[17] A.A. Mekonen, A.B. Berlie, M.B. Ferede, Spatial and temporal drought incidence analysis in the northeastern highlands of Ethiopia, Geoenviron Disasters 7 (2020) 10, https://doi.org/10.1186/s40677-020-0146-4.
[18] S.B. Wassie, D.A. Mengistu, A.B. Berlie, Trends and spatiotemporal patterns of meteorological drought incidence in North Wollo, northeastern highlands of Ethiopia, Arabian J. Geosci. 15 (2022) 1158.
[19] E. Gebre, G. Berhan, A. Lelago, Application of remote sensing and GIS to characterize agricultural drought conditions in North Wollo zone, Amhara regional state, Ethiopia, J. Nat. Sci. Res. (2017).
[20] A. Senamaw, S. Addisu, K.V. Suryabhagavan, Mapping the spatial and temporal variation of agricultural and meteorological drought using geospatial techniques, Ethiopia, Environ Syst Res 10 (2021) 15, https://doi.org/10.1186/s40068-020-00204-2.
[21] S. Dogan, A. Berktay, V.P. Singh, Comparison of multi-monthly rainfall-based drought severity indices, with application to semi-arid Konya closed basin, Turkey, J. Hydrol. 470–471 (2012) 255–268, https://doi.org/10.1016/j.jhydrol.2012.09.003.
[22] D. Ayalew, K. Tesfaye, G. Mamo, B. Yitaferu, W. Bayu, Variability of rainfall and its current trend in Amhara region, Ethiopia, Afr. J. Agric. Res. 7 (2012) 1475–1486.
[23] A.E. Harka, N.B. Jilo, F. Behulu, Spatial-temporal rainfall trend and variability assessment in the Upper Wabe Shebelle River Basin, Ethiopia: application of innovative trend analysis method, J. Hydrol.: Reg. Stud. 37 (2021) 100915, https://doi.org/10.1016/j.ejrh.2021.100915.
[24] G. Tsakiris, Drought risk assessment and management, Water Resour Manage 31 (2017) 3083–3095, https://doi.org/10.1007/s11269-017-1698-2.
[25] Y.-A. Liou, G.M. Mulualem, Spatio–temporal assessment of drought in Ethiopia and the impact of recent intense droughts, Rem. Sens. 11 (2019) 1828, https://doi.org/10.3390/rs11151828.
[26] EIAR, Ethiopian Inistitute of Agricultural Reasearch, Coordination of National Agricultural Research System, Ethiopia. English and Amharic Version, EIAR, Addis Ababa, 2011, p. pp137.
[27] D. Gorfu, E. Ahmed, Crops and Agro-Ecological Zones of Ethiopia, Ethiopian Institute of Agricultural Research, 2012.
[28] L. Silici, Agroecology: what it Is and what it Has to Offer, Issue Paper 14629IIED, International Institute for Environment and Development, London, 2014.
[29] CSA, Population Projection of Ethiopia for All Regions from 2014 – 2017, CSA, Addis Ababa, Ethiopia, 2013.
[30] M.M. Alemu, G.T. Bawoke, Analysis of spatial variability and temporal trends of rainfall in Amhara region, Ethiopia, Journal of Water and Climate Change 11 (2020) 1505–1520, https://doi.org/10.2166/wcc.2019.084.
[31] T. Dinku, C. Funk, P. Peterson, R. Maidment, T. Tadesse, H. Gadain, P. Ceccato, Validation of the CHIRPS satellite rainfall estimates over eastern Africa, Quart J Royal Meteoro Soc 144 (2018) 292–312, https://doi.org/10.1002/qj.3244.
[32] S. Caparoci Nogueira, M. Moreira, M. Lordelo Volpato, Evaluating precipitation estimates from eta, TRMM and CHRIPS data in the south-southeast region of minas gerais state—Brazil, Rem. Sens. 10 (2018) 313, https://doi.org/10.3390/rs10020313.
[33] C. Funk, P. Peterson, M. Landsfeld, D. Pedreros, J. Verdin, S. Shukla, G. Husak, J. Rowland, L. Harrison, A. Hoell, J. Michaelsen, The climate hazards infrared precipitation with stations—a new environmental record for monitoring extremes, Sci. Data 2 (2015) 150066, https://doi.org/10.1038/sdata.2015.66.
[34] M.-T. Sattari, A. Rezazadeh-Joudi, A. Kusiak, Assessment of different methods for estimation of missing data in precipitation studies, Nord. Hydrol 48 (2017) 1032–1044, https://doi.org/10.2166/nh.2016.364.
[35] L.V. Duarte, K.T.M. Formiga, V.A.F. Costa, Comparison of methods for filling daily and monthly rainfall missing data: statistical models or imputation of satellite retrievals? Water 14 (2022) 3144, https://doi.org/10.3390/w14193144.
[36] C. Yozgatligil, S. Aslan, C. Iyigun, I. Batmaz, Comparison of missing value imputation methods in time series: the case of Turkish meteorological data, Theor. Appl. Climatol. 112 (2013) 143–167, https://doi.org/10.1007/s00704-012-0723-x.
[37] M. Egigu, Techniques of filling missing values of daily and monthly rain fall data: a review, SF J Environ Earth Sci 3 (1) (2020) 1036, 2020.
[38] E.L. Goshu, S. Upadhyaya, R. Ramsankaran, Meteorological Drought Monitoring across Different Rainfall Regimes of Ethiopia Using Chirps V2-Rainfall Data, 2017.
[39] M. Taye, D. Sahlu, B.F. Zaitchik, M. Neka, Evaluation of satellite rainfall estimates for meteorological drought analysis over the upper blue nile basin, Ethiopia, Geosciences 10 (2020) 352, https://doi.org/10.3390/geosciences10090352.
[40] S. Upadhyaya, R. Ramsankaran, Modified-INSAT multi-spectral rainfall algorithm (M-IMSRA) at climate region scale: development and validation, Remote Sensing of Environment 187 (2016) 186–201, https://doi.org/10.1016/j.rse.2016.10.013.
[41] G.T. Diro, D.I.F. Grimes, E. Black, A. O'Neill, E. Pardo-Iguzquiza, Evaluation of reanalysis rainfall estimates over Ethiopia, Intl Journal of Climatology 29 (2009) 67–78, https://doi.org/10.1002/joc.1699.
[42] R.I. Maidment, D. Grimes, R.P. Allan, E. Tarnavsky, M. Stringer, T. Hewison, R. Roebeling, E. Black, The 30 year TAMSAT African rainfall climatology and time series (TARCAT) data set, J. Geophys. Res. Atmos. 119 (10) (2014), 619-10,644.
[43] B. Ratner, The correlation coefficient: its values range between +1/−1, or do they? J Target Meas Anal Mark 17 (2009) 139–142, https://doi.org/10.1057/jt.2009.5.
[44] M. Gocic, S. Trajkovic, Analysis of changes in meteorological variables using Mann-Kendall and Sen's slope estimator statistical tests in Serbia, Global Planet. Change 100 (2013) 172–182, https://doi.org/10.1016/j.gloplacha.2012.10.014.
[45] S.M. Pingale, D. Khare, M.K. Jat, J. Adamowski, Spatial and temporal trends of mean and extreme rainfall and temperature for the 33 urban centers of the arid and semi-arid state of Rajasthan, India, Atmos. Res. 138 (2014) 73–90, https://doi.org/10.1016/j.atmosres.2013.10.024.
[46] Y. Wang, Y. Xu, H. Tabari, J. Wang, Q. Wang, S. Song, Z. Hu, Innovative trend analysis of annual and seasonal rainfall in the Yangtze River Delta, eastern China, Atmos. Res. 231 (2020) 104673, https://doi.org/10.1016/j.atmosres.2019.104673.
[47] F. Fentaw, A.M. Melesse, D. Hailu, A. Nigussie, Precipitation and streamflow variability in Tekeze River basin, Ethiopia, in: Extreme Hydrology and Climate Variability, Elsevier, 2019, pp. 103–121, https://doi.org/10.1016/B978-0-12-815998-9.00010-5.
[48] A.S. Yusuf, C.O. Edet, C.O. Oche, E.P. Agbo, Trend Analysis of Temperature in Gombe State Using Mann Kendall Trend Test, 2018.
[49] T.T. Zeleke, F. Giorgi, G.T. Diro, B.F. Zaitchik, Trend and periodicity of drought over Ethiopia, Intl Journal of Climatology 37 (2017) 4733–4748, https://doi.org/10.1002/joc.5122.
[50] S. Yue, C. Wang, The mann-kendall test modified by effective sample size to detect trend in serially correlated hydrological series, Water Resour. Manag. 18 (2004) 201–218, https://doi.org/10.1023/B:WARM.0000043140.61082.60.
[51] M. Achite, T. Caloiero, A. Wał, N. Krakauer, Analysis of the spatiotemporal annual rainfall variability in the wadi cheliff basin (Algeria) over the period 1970 to 2018, Water 13 (2021) 1–9, https://doi.org/10.3390/w13111477.
[52] A. Asfaw, B. Simane, A. Hassen, A. Bantider, Variability and time series trend analysis of rainfall and temperature in northcentral Ethiopia: a case study in Woleka sub-basin, Weather Clim. Extrem. 19 (2018) 29–41, https://doi.org/10.1016/j.wace.2017.12.002.
[53] C.M. Dunning, E.C. Black, R.P. Allan, The onset and cessation of seasonal rainfall over Africa, J. Geophys. Res. Atmos. 121 (11) (2016), 405-411,424.

[54] O.F. Ati, C.J. Stigter, E.O. Oladipo, A comparison of methods to determine the onset of the growing season in northern Nigeria, Intl Journal of Climatology 22 (2002) 731–742, https://doi.org/10.1002/joc.712.
[55] B. Liebmann, I. Bladé, G.N. Kiladis, L.M.V. Carvalho, G.B. Senay, D. Allured, S. Leroux, C. Funk, Seasonality of african precipitation from 1996 to 2009, J. Clim. 25 (2012) 4304–4322, https://doi.org/10.1175/JCLI-D-11-00157.1.
[56] W.J. Gibbs, J.V. Maher, Rainfall Deciles Drought Inddicators, 1967.
[57] E. Asrari, M. Masoudi, E. Afrough, Analyzing spatial and temporal pattern of humid, normal and drought years using percent of normal precipitation index (pnpi) in Fars province, Iran, J. Appl. Sci. Environ. Sanit. 6 (2011) 299–308.
[58] WMO, World Metrological Organization, With Svoboda, M. Hayes, D. M Wood, Standardized Precipitation Index User, 2012. Geneva, Switzerland WMO-No. 1090.
[59] H.A. Okal, F.K. Ngetich, J.M. Okeyo, Spatio-temporal characterisation of droughts using selected indices in Upper Tana River watershed, Kenya, Scientific African 7 (2020) e00275, https://doi.org/10.1016/j.sciaf.2020.e00275.
[60] S.M. Vicente-Serrano, S. Beguería, J.I. López-Moreno, A multiscalar drought index sensitive to global warming: the standardized precipitation evapotranspiration index, J. Clim. 23 (2010) 1696–1718, https://doi.org/10.1175/2009JCLI2909.1.
[61] S. Beguería, S.M. Vicente-Serrano, F. Reig, B. Latorre, Standardized precipitation evapotranspiration index (SPEI) revisited: parameter fitting, evapotranspiration models, tools, datasets and drought monitoring, Int. J. Climatol. 34 (2014) 3001–3023, https://doi.org/10.1002/joc.3887.
[62] C. Chortaria, C.A. Karavitis, S. Alexandris, Development of the SPI Drought Index for Greece Using Geo-Statistical Methods, BALWOIS 2010-Ohrid, Republic of Macedonia, 2010, 25-29 May 2010.
[63] T.B. McKee, N.J. Doesken, J. Kleist, The Relationship of Drought Frequency and Duration to Time Scales, 1993, pp. 179–183. Boston.
[64] L. Gonfa, Climate Classification of Ethiopia, National Meteorological Service Agency (NMA), Ethiopia, 1996.
[65] K.V. Suryabhagavan, GIS-based climate variability and drought characterization in Ethiopia over three decades, Weather Clim. Extrem. 15 (2017) 11–23, https://doi.org/10.1016/j.wace.2016.11.005.
[66] C.D. Geleta, T.A. Deressa, Evaluation of climate hazards Group InfraRed precipitation station (CHIRPS) satellite-based rainfall estimates over finchaa and neshe watersheds, Ethiopia, Engineering Reports 3 (2021) e12338, https://doi.org/10.1002/eng2.12338.
[67] Y. Bayissa, T. Tadesse, G. Demisse, A. Shiferaw, Evaluation of satellite-based rainfall estimates and application to monitor meteorological drought for the upper blue nile basin, Ethiopia, Rem. Sens. 9 (2017) 669, https://doi.org/10.3390/rs9070669.
[68] D.P.S. Terêncio, L.F. Sanches Fernandes, R.M.V. Cortes, J.P. Moura, F.A.L. Pacheco, Rainwater harvesting in catchments for agro-forestry uses: a study focused on the balance between sustainability values and storage capacity, Sci. Total Environ. 613–614 (2018) 1079–1092, https://doi.org/10.1016/j.scitotenv.2017.09.198.
[69] A. Alemayehu, M. Maru, W. Bewket, M. Assen, Spatiotemporal variability and trends in rainfall and temperature in Alwero watershed, western Ethiopia, Environ Syst Res 9 (2020) 22, https://doi.org/10.1186/s40068-020-00184-3.
[70] W.H. Cheung, G.B. Senay, A. Singh, Trends and spatial distribution of annual and seasonal rainfall in Ethiopia, Intl Journal of Climatology 28 (2008) 1723–1734, https://doi.org/10.1002/joc.1623.
[71] W. Bewket, D. Conway, A note on the temporal and spatial variability of rainfall in the drought-prone Amhara region of Ethiopia, Intl Journal of Climatology 27 (2007) 1467–1477, https://doi.org/10.1002/joc.1481.
[72] T.G. Asaminew, A. Araya, G. Atkilt, H. Solomon, Modelling the potential impact of climate change on cotton (Gossypium hirsutum) production in northeastern semi-arid Afar and western Tigray regions of Ethiopia, J Earth Sci Clim Change 8 (2017) 1–7.
[73] D. Ademe, B.F. Zaitchik, K. Tesfaye, B. Simane, G. Alemayehu, E. Adgo, Climate trends and variability at adaptation scale: patterns and perceptions in an agricultural region of the Ethiopian Highlands, Weather Clim. Extrem. 29 (2020) 100263, https://doi.org/10.1016/j.wace.2020.100263.
[74] A.S.T. de la Poterie, W.E. Jjemba, R. Singh, E.C. de Perez, C.V. Costella, J. Arrighi, Understanding the use of 2015–2016 El Niño forecasts in shaping early humanitarian action in Eastern and Southern Africa, Int. J. Disaster Risk Reduc. 30 (2018) 81–94.
[75] C. Em-dat, The OFDA/CRED International Disaster Database. 2001, Université Catholique de Louvain, Belgium, 2013.
[76] K. Winkler, U. Gessner, V. Hochschild, Identifying droughts affecting agriculture in africa based on remote sensing time series between 2000–2016: rainfall anomalies and vegetation condition in the context of ENSO, Rem. Sens. 9 (2017) 831, https://doi.org/10.3390/rs9080831.